UT GSBS Dissertations and Theses (Open Access)   Graduate School of Biomedical Sciences

5-2010

TYPE I INSULIN-LIKE GROWTH FACTOR RECEPTOR TYROSINE KINASE AS A MOLECULAR TARGET IN MANTLE CELL LYMPHOMA

Deeksha Vishwamitra

Follow this and additional works at: http://digitalcommons.library.tmc.edu/utgsbs_dissertations

Part of the Medical Pathology Commons

Recommended Citation

The TMC LIBRARY
Health Sciences Resource Center

TYPE I INSULIN-LIKE GROWTH FACTOR RECEPTOR TYROSINE KINASE AS A

MOLECULAR TARGET IN MANTLE CELL LYMPHOMA

A

THESIS

Presented to the Faculty of
The University of Texas
Health Science Center at Houston
and
The University of Texas
M. D. Anderson Cancer Center
Graduate School of Biomedical Sciences

in Partial Fulfillment

of the Requirements

for the Degree of

MASTER OF SCIENCE

by

Deeksha Vishwamitra, B.S.
Houston, Texas

May 2010

Dedications

To my amazing parents, thank you for always

exemplifying the true embodiment of unconditional

greatness

I love you forever and always

Acknowledgements

Firstly, I would like to sincerely thank my supervisor and mentor, Dr. Hesham Amin, who took the time to guide, teach, and lead me through the first years of my career. Thank you for your encouragement, patience, and belief in my abilities as a scientist. I have learned many things working in your lab and have gained the confidence to endure the scientific world through your lessons.

Next, I would like to thank the members of the lab: Ping Shi, Yong Li, and Bin Shi, who are all talented postdoctoral fellows. Thank you for answering my numerous questions about science every day. I have learned how to be an independent scientific thinker by watching you.

I would like to truly thank the members of my supervisory committee: Dr. Russell Broaddus, Dr. Joya Chandra, Dr. Joseph Ludwig, and Dr. Patrick Zweidler-McKay. You have been with me since the beginning and I owe my progress to your advice and encouragement.

I could not accomplish my scientific dreams without the Graduate School of Biomedical Sciences. Thank you for giving me the opportunity to work in an atmosphere where I can learn everyday by being around the best mentors and thank you for making my graduate school experience wonderful.

Lastly, I would like to thank my family for all their love, support, and understanding through all my endeavors. I could not have done this without you.

Type I Insulin-Like Growth Factor Receptor Tyrosine Kinase as a Molecular Target in Mantle Cell Lymphoma

Deeksha Vishwamitra, B.S.

Supervisory Advisor: Hesham M. Amin, M.D.

Mantle cell lymphoma (MCL) is an aggressive B-cell lymphoid malignancy representing 5-10% of all non-Hodgkin's lymphomas. It is distinguished by the t(11;14)(q13;q32) chromosomal translocation that juxtaposes the proto-oncogene *CCND1*, which encodes cyclin D1 at 11q13 to the *IgH* gene at 14q32. MCL patients represent about 6% of all new cases of Non-Hodgkin's lymphomas per year or about 3,500 new cases per year. MCL occurs more frequently in older adults – the average age at diagnosis is the mid-60s with a male-to-female ratio of 2-3:1. It is typically characterized by the proliferation of neoplastic B-lymphocytes in the mantle zone of the lymph node follicle that have a prominent inclination to disseminate to other lymphoid tissues, bone marrow, peripheral blood and other organs. MCL patients have a poor prognosis because they develop resistance/relapse to current non-specific therapeutic regimens. It is of note that the exact molecular mechanisms underlying the pathogenesis of MCL are not completely known. It is reasonable to anticipate that better characterization of these mechanisms could lead to the development of specific and likely more effective therapeutics to treat this aggressive disease. The type I insulin-like growth factor receptor (IGF-IR) is thought to be a key player in several different solid malignancies such as those of the prostate, breast, lung, ovary, skin and soft tissue. In addition, recent studies in our lab showed evidence to support a pathogenic role of IGF-IR in some types of T-cell lymphomas and chronic myeloid leukemia. Constitutively active IGF-IR induces its oncogenic effects through the inhibition of apoptosis and induction of transformation, metastasis, and angiogenesis. Previous studies have shown that signaling through IGF-IR leads to the

v

activation of multiple signaling transduction pathways mediated by the receptor-associated tyrosine kinase domain. These pathways include PI3K/Akt, MAP kinase, and Jak/Stat. In the present study, we tested the possible role of IGF-IR in MCL. Our results demonstrate that IGF-IR is over-expressed in mantle cell lymphoma cell lines compared with normal peripheral blood B-lymphocytes. Furthermore, inhibition of IGF-IR by the cyclolignan picropodophyllin (PPP) decreased cell viability and cell proliferation in addition to induction of apoptosis and G2/M cell cycle arrest. Screening of downstream oncogenes and apoptotic proteins that are involved in both IGF-IR and MCL signaling after treatment with PPP or IGF-IR siRNA showed significant alterations that are consistent with the cellular changes observed after PPP treatment. Therefore, our findings suggest that IGF-IR signaling contributes to the survival of MCL and thus may prove to be a legitimate therapeutic target in the future.

Table of Contents

List of Illustrations

Chapter I: Introduction and Background

1.1 Mantle Cell Lymphoma

Mantle cell lymphoma (MCL) is an aggressive B-cell lymphoid neoplasm representing 5-10% of all non-Hodgkin's lymphomas. Almost all cases of MCL have a genetic change that is distinguished by the t(11;14)(q13;q32) chromosomal translocation and is considered the primary genetic event. This translocation juxtaposes the proto-oncogene *CCND1*, which encodes cyclin D1 at chromosome 11q13 to the *IgH* gene at chromosome 14q32 (1) (**Figure 1**).
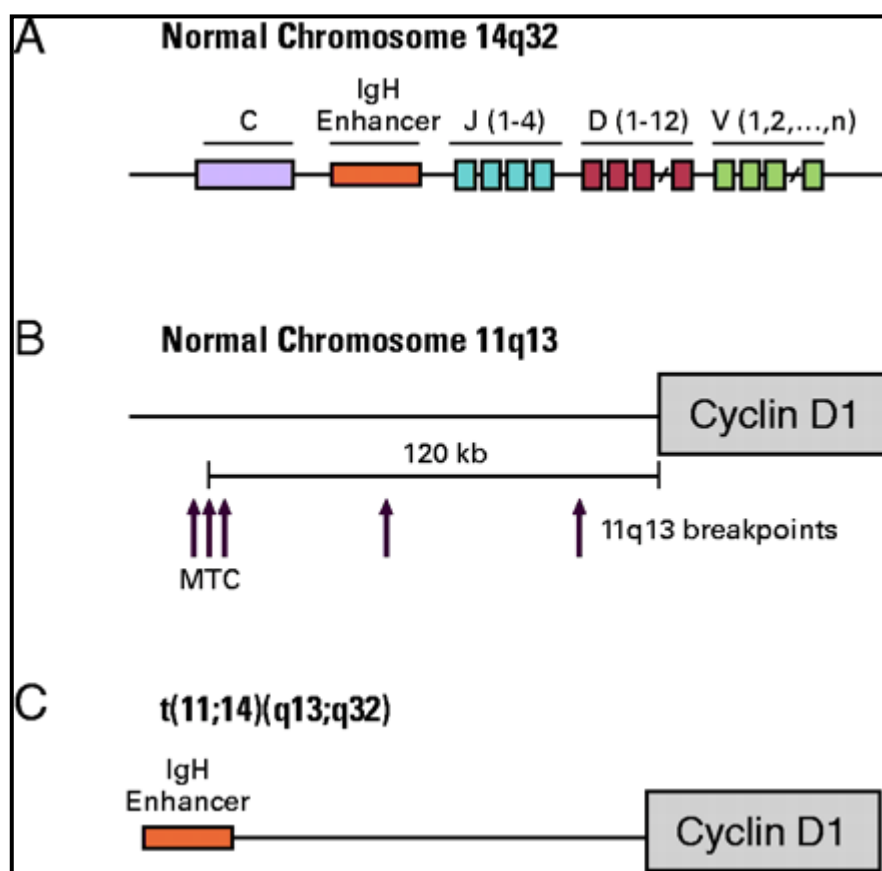
Figure 1: (A) Representation of a normal *IgH* gene. The IgH enhancer is separated by the constant {C} region and the joining {J}, diversity {D}, and variable {V} regions. J, D, and V undergo recombination to produce unique immunoglobulins during normal B-lymphocyte development. **(B)** Represtantion of normal *CCND1* gene encoding cyclin D1. It contains several breakpoint cluster regions, including the major translocation cluster (MTC). **(C)** Translocation results in *CCND1* being brought under the control of *IgH* enhancer initiating the onset of MCL. Adapted from Fernandez,V. et al: J Clin Oncol Vol. 23, 2005: 6364-6369. Reprinted with permission. © 2008 American Society of Clinical Oncology. All rights reserved.

A normal *IgH* gene, located at chromosome 14q32, includes two regions that contain genes that specify antibodies called the constant region (C) and the variable region (V). The variable region is composed of three segments V, D, and J, which undergo a series of recombinations to produce a unique set of immunoglobulins. The *IgH* enhancer is located between the constant region and variable region (**Figure 1A**).

The normal *CCND1* gene, located at chromosome 11q13, encodes the cell cycle regulatory protein cyclin D1. It also encompasses several breakpoint regions, including the major translocation cluster (MTC), in which the translocation that takes place in MCL most likely occurs (**Figure 1B**). It is thought that in MCL, during B-lymphocyte development in the outer edge of the lymph node follicle (mantle zone), a break in chromosome 11 results in the transfer of a small segment of chromosome 11 to chromosome 14, resulting in a genetic exchange of chromosomal segments. During this process, *CCND1* is brought under the control of the *IgH* enhancer which causes the lymphocyte to overproduce cyclin D1, a protein that facilitates cell division at the G1/S transition phase (cyclin D1 is not normally expressed in normal B-lymphocytes) (1) (**Figure 1C**). An accumulation of these altered B-lymphocytes in the mantle zone is a characteristic event in mantle cell lymphoma. This event most likely occurs during early B cell stage differentiation, where the cell is undergoing gene rearrangement with the recombination of the VDJ segments by means of double strand breaks (2).

The neoplastic MCL lymphocytes, which express antigens that are normally detected in naïve B cells like T-cell associated CD5, are typically characterized by a prominent inclination to disseminate to other lymphoid tissues, bone marrow, peripheral blood and other organs. Most likely, the selective oncogenic advantage of the t(11;14) translocation fully develops when these cells enter the differentiation state of a mature naïve pre-germinal center B cell (3). This alteration is thought to be the primary event in

3

MCL pathogenesis, perhaps leading to deregulation of the cell cycle at the G1/S phase transition (1, 3).

The alteration in the G1/S phase transition results in the hyperphosphorylation of the retinoblastoma 1 (Rb1) protein by cyclinD1/CDK4 and cyclin D1/CDK6 complexes, causing the E2F transcription factors to be released and allowing for entry into the S phase of the cell cycle (1, 3).

In addition to Rb1 hyperphosphorylation, cyclin D1 also plays a role in the late G1/S transition by deregulating the cyclin E/CDK2 complex and the CDK inhibitor p27 (1). MCL cells degrade p27 by the proteosome pathway, thereby inhibiting the protein from inducing cell cycle arrest (1, 3). This, in turn, would result in an overactive cyclin E-CDK2 complex to also assist in p27 degradation.

The overexpression of cyclin D1 is the distinguishing feature of MCL, however, it is not exclusive since it has been less frequently seen in other hematological malignancies such as hairy cell leukemia and plasma cell myeloma as well as in breast, small cell lung, renal carcinomas, and soft tissue sarcoma (1, 4-8).

When the disease progresses into more advanced stages, MCL tumor cells acquire a high number of secondary chromosomal and molecular alterations in proteins that normally function in regulating the cell cycle and growth arrest (BMI1, INK4a, ARF/P53, CDK4/cyclin E and RB1). Additionally, gain of function or loss of function mutations interfere in normal activity of DNA damage response proteins [ataxia telangiectasia mutated gene (*ATM*), checkpoint homolog kinase 2 (CHK2) and p53] as well as cell survival pathways (1). The CDKN2A locus on chromosome 9p21 encodes for the CDK4 inhibitor INK4a and the p53 regulator ARF (3). In normal cells, CDK4 and CDK6 are inhibited by INK4a, causing Rb1 protein to be in its anti-proliferative state. Homozygous deletions for this locus have been detected in some MCL cases, thereby causing Rb1 to become hyperphosphorylated. This, in combination with the overexpression of cyclin D1, might

further assist the transition of the tumorigenic cells into the next phase of the cell cycle (3). A deletion at this locus also affects ADP ribosylation factor (ARF) protein, which stabilizes p53 by preventing degradation by MDM2. ARF instability causes deregulation of p53, allowing entry into the S phase of the cell cycle.

The most frequent alteration that occurs in DNA damage response pathways is the deletion in the chromosomal region 11q22-23, which includes *ATM* (1). *ATM* mutations have been detected in 40-75% of MCL cases. Normally, *ATM* functions to assist cells in recognizing broken DNA strands that are damaged by harmful agents such as toxic chemicals, radiation, or the natural exchange of genetic material during cell division (9). The ATM protein coordinates efficient DNA repair by activating enzymes that fix the broken strands, thereby maintaining the stability of DNA.

Lastly, mutations in other DNA damage response pathways, such as CHK1 and CHK2 checkpoint kinases also allow unguarded entry into the next phase of the cell cycle. MCL also shows amplification of anti-apoptotic protein Bcl-2 and deletions of pro-apoptotic protein BIM, although this aspect is not well studied (3). A constitutively active PI3K/Akt pathway also contributes to the pathogenesis of MCL and preferentially occurs in blastoid variants. The presence of phosphorylated/active Akt in primary MCL cases was associated with the inactivation of p27 (CDK inhibitor) and phosphorylation of forkhead box O3a (FOXO3a), MDM2, Bad, mammalian target of rapamycin (mTOR), and p70S6K. Inhibiting this pathway in MCL cell lines upregulated p27 and reduced the phosphorylation of Akt, FOXO3a, MDM2, Bad, and mTOR. These observations were found through the loss of PTEN expression. PTEN normally functions to inhibit the activation of phosphatidylinositol (3,4,5)-trisphosphate (PIP3), an activator of the PI3K/Akt pathway (10).

Although a definite model for the pathogenesis of MCL has not been elucidated, a proposed model shows the progression from the occurrence of the initial translocation in

the early stages, then the accumulation of several secondary alterations in the later stages, which ultimately lead into the final advanced phase of the disease (3).

Almost all cases of MCL carry the t(11;14) translocation, except for a small subset of MCL tumors that are negative for cyclin D1. In these tumors, it was found that there was an overexpression of cyclin D2 or cyclin D3 in addition to another chromosomal translocation t(2;12)(p11;p13), which juxtaposes cyclin D2 and the kappa immunoglobulin light chain (3) . However, these mechanisms are not well understood.

Clinically, MCL patients represent about 3,500 new cases per year (11, 12). MCL occurs more frequently in older adults , the average age at diagnosis is the mid-60s and is more prevalent in males. MCL patients have a poor prognosis because they develop resistance/relapse to current non-specific therapeutic regimens. Current treatments include chemotherapy combinations plus rituximab (R), a monoclonal antibody that specifically targets the CD20 antigen which is present on the surface of B-lymphocytes (11-13). These combinations include R-CHOP [Cyclophosphamide (also called Cytoxan/Neosar), Doxorubicin (Adriamycin), Vincristine (Oncovin) and Prednisolone] and more aggressive treatments such as R-HyperCVAD (Cyclophosphamide, Vincristine, Doxorubicin, Dexamethasone), and R-FCM (Fludarabine, Cyclophosphamide, Mitoxantrone) (11-13). Other approaches include radioimmunotherapy combinations with rituximab, proteosome inhibitors such as Velcade, and stem cell transplantations (**Figure 2**).

In spite of all the recent efforts made to better understand the molecular mechanisms underlying MCL, deciphering the exact pathogenesis of this disease still proves to be extremely challenging, and therefore is still not completely known. Current treatment approaches are non-curative and the corresponding survival curves are characterized by a delayed, but continuous decline and a median survival of 4 to 6 years. It is reasonable to anticipate that better characterization of these mechanisms could lead to

the development of specific and likely more effective therapeutics to treat this highly

aggressive disease.

New untreated mantle cell lymphoma

Not transplant eligible → Chemotherapy → Response → Relapse → Other chemoRx / R-thalidomide / mTOR inhibitor / Proteosome inhibitor

Transplant eligible → R-hyperCVAD → < CR → Transplant / CR → Observe ; R-CHOP → Response → Transplant
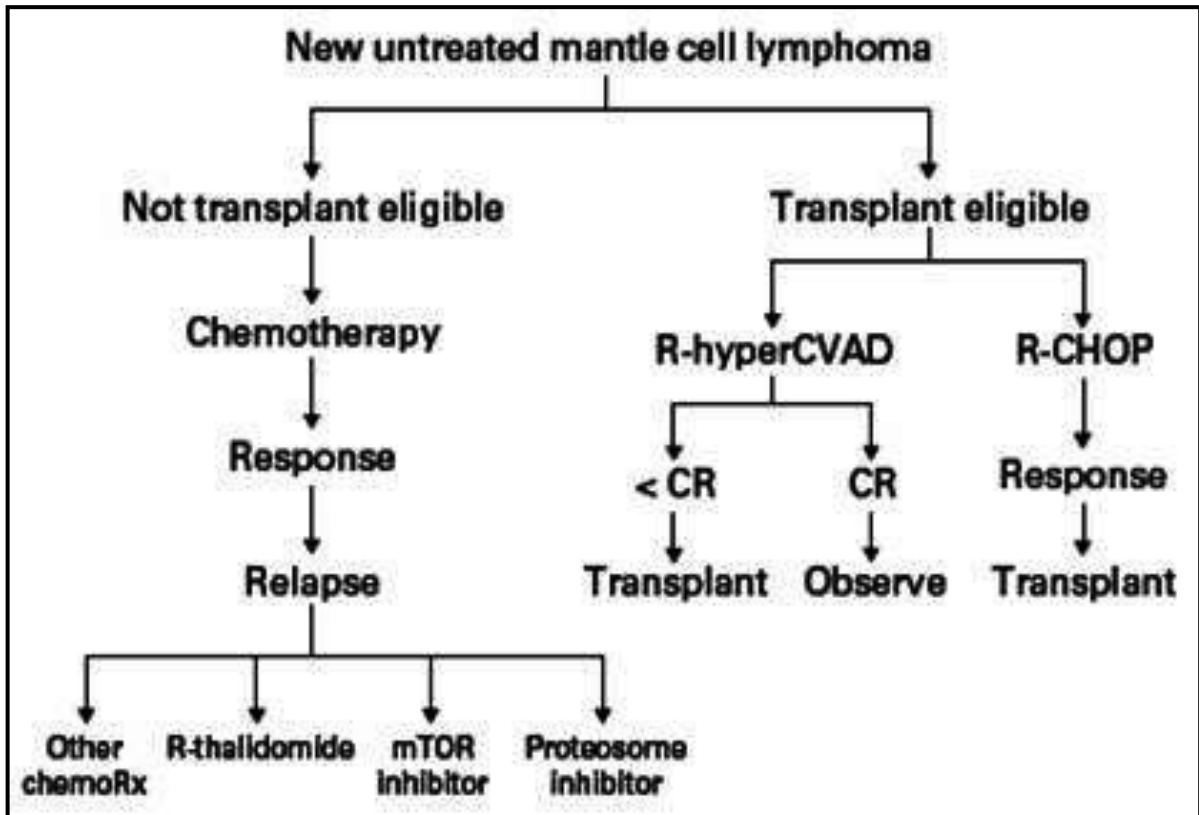
Figure 2: Current treatment approaches for MCL. Adapted from Witzig, T.E. et al: J Clin Oncol Vol 23, 2005: 6409-6414. Reprinted with permission. © 2008 American Society of Clinical Oncology. All rights reserved.

1.3 Overview of the insulin-like growth factor system

The insulin–like growth factor (IGF) system plays significant roles in both embryonic and postnatal development as well as important functions in normal adult physiology. The IGF system includes 4 receptors: type I insulin-like growth factor receptor I (IGF-IR), IGF-IIR, insulin receptor (IR), and the hybrid receptors (HR) consisting of one-half IR and one-half IGF-IR. These have been shown to interact with at least three ligands: IGF-I, IGF-II, and insulin (**Figure 3**). IR, IGF-IR, and IGF-IIR have strongest binding affinity for their respective ligand, whereas binding of insulin to IGF-IR and IGF-I to IR are approximately 100-fold less. Both IGF-I and IGF-II signaling is mediated through IGF-IR, however, IGF-I has a 4-5-fold higher binding affinity. The IGF family also includes 6 regulatory proteins called IGF binding proteins 1-6 that regulate IGF signaling (14).
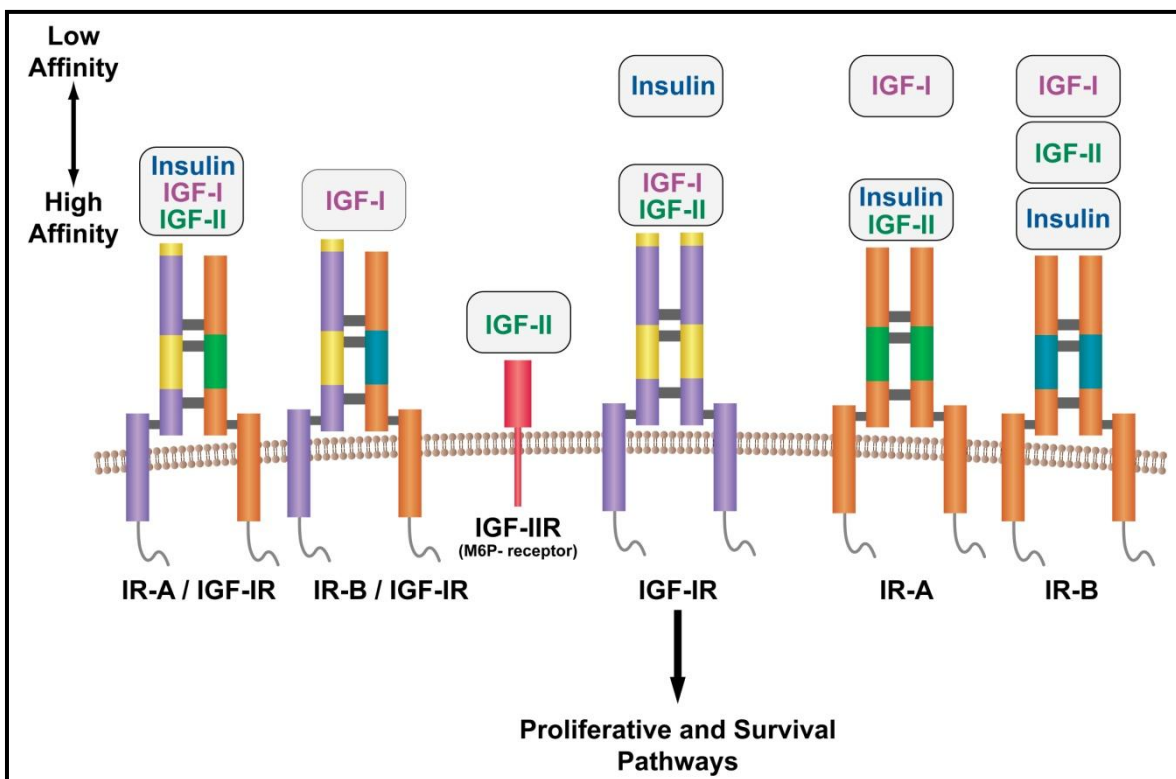
Figure 3: Overview of IGF system: The IGF system consists of 4 receptors: IGF-IR, IGF-IIR, IR, and HR. These receptors have been shown to interact with at least three ligands: IGF-1, IGF-II, and insulin. In addition, the IGF system also includes 6 regulatory proteins called IGF binding proteins 1-6 that regulate IGF signaling.

1.4 IGF-I

IGF-I is a single chain peptide that has 62% homology with each IGF-II and 40% homology with proinsulin (14). Evidence shows that IGF-I is synthesized in a variety of tissues and cultured cell types, suggesting that the protein may have autocrine or paracrine effector functions, unlike insulin which is stored within cells of a particular tissue (pancreas) and has mainly autocrine effects (15-19). Liver secretion of IGF-I is regulated by growth hormone (GH) which signals peripheral tissues to grow, whereas insulin is tightly regulated by glucose uptake (18, 20, 21). Therefore, insulin is primarily associated with inducing metabolic effects, whereas the IGF-I is essential a growth factor and an anabolic agent.

IGF-I is the primary ligand for IGF-IR. There is increasing evidence that IGF-I might provide a major link between IGF-IR and the development of cancers through its influence on the regulation of normal cell proliferation, differentiation and apoptosis. Although most cancers do not secrete IGF-I, high concentrations of circulating IGF-I in serum appear to contribute to the growth, maintenance and progression of the most common cancers, including cancers of the breast, lung and colon (22-26). For example, previous studies have demonstrated that colonic epithelium in acromegalic patients is characterized by increased proliferation which is proportional to serum IGF-I levels (27). Also, there is a large amount of evidence from both *in vitro* and *in vivo* experiments that prostate cancer is mitogenically responsive to IGF-I (23). Several mouse models have shown reduced proliferation of androgen-dependent prostate cancer cells in IGF-I deficient hosts relative to control hosts, testifying to the strong mitogenic properties of IGF-I.

IGF-I appears to tightly control both positive and negative regulators of the cell cycle primarily through the interaction with IGF-IR. It has been previously documented that IGF-I increases cell proliferation by amplifying DNA synthesis and upregulating cyclin D1 mRNA expression, which allows entry into the S phase of the cell cycle. In a study using skeletal myoblasts, it was demonstrated that the early effects of IGF-I during cell cycle progression

9

are associated with the stabilization of Rb1 phosphorylation that is typical of proliferating cells. It then upregulates CDK4 and cyclin D1 gene expression which further maintain Rb1 phosphorylation (22). In another study using neocortical neural progenitor cells, *in vitro* addition of IGF-I induced rapid increase in cyclin D1 and cyclin D3 . This led to a further increase in cyclin E, which also assists in the G1/S phase transition. Simultaneously, observed decrease in CDK inhibitors p27 and p57 suggested that downregulation of negative regulators of cell cycle also contributes to the mitogenesis induced by IGF-I. These effects were further demonstrated *in vivo*, where injection of IGF-I led to increased DNA synthesis and number of S phase cells, with simultaneous increase in phosphorylated/activated Akt, cyclin D1 and cyclin E (28). Endogenous blockade of IGF-I with an anti-IGF-I antibody led to decreased DNA synthesis, upregulation of p27 and p57, as well as prevention of cyclin E mRNA expression. Interestingly, it has been demonstrated that the effects exerted by IGF-I are primarily induced through the PI3K/Akt pathway. Blocking this pathway, but not the MAPK/Erk pathway, inhibited the mitogenic potential of IGF-I (28). This data suggests strong mitogenic potential of IGF-I, acting essentially through IGF-IR.

1.5 IGF-IR

1.5 a. Regulation of IGF-IR gene expression

IGF-IR gene is located at chromosome 15q25-15q26 and is regulated by several

different stimuli including hormones, growth factors, and nutritional status (29). For

example, in addition to its stimulatory effects on IGF-IR, it has also been shown that high

IGF-I levels result in a decrease of receptor number, suggesting that IGFs may act as

negative regulators of a positive feedback mechanism (18, 29, 30). Furthermore, it has

been shown that other growth factors, hormones, and transcription factors such as AP-1,

SP-1, fibroblast growth factor (FGF), platelet-derived growth factor (PDGF), epidermal

growth factor (EGF), estrogens, glucocorticoids, and GH stimulate IGF-IR expression,

whereas WT1 (Wilms tumor 1 protein) and STAT1 inhibit the expression of IGF-IR (30-34).

Additionally, wild type p53 inhibits IGF-IR expression, in contrast to mutated p53 which has

stimulatory effects on IGF-IR activity without binding to its promoter. The transcriptional

role of WT1 appears to depend on the cellular status of p53. WT1 can inhibit IGF-IR only in

the presence of wild type p53. It has been illustrated previously that several colorectal and

breast cancer specimens with elevated IGF-IR levels demonstrated coexpression of WT1

and mutated p53, suggesting a possible sequestration of WT1 by mutated p53 (22, 34).

1.5 b. IGF-IR structure and signaling

IGF-IR is a receptor tyrosine kinase consisting of two identical α subunits and two

identical β subunits that are connected by disulfide bridges to form the functional

homodimeric receptor complex. The α subunit is entirely extracellular and contains a

cysteine rich domain that forms the primary binding site for its ligands IGF-I and, to a lesser

affinity, IGF-II and insulin. The β subunit includes an extracellular domain, a 24-residue

hydrophobic transmembrane domain, and a larger cytoplasmic region which shares 84%

homology to the insulin receptor (30, 35). Tyrosine 950 is the binding site for its substrates,

insulin receptor substrates 1-4 (IRS-1-4) and src homology and collagen (shc) domain protein, among others. The intracellular region of the β subunit contains an ATP binding site at lysine 1003. It also contains a kinase domain encompassing the activation loop made up of three critical tyrosines at positions 1131, 1135, and 1136, which become phosphorylated upon ligand binding. Residue 1136 is particularily important in that it maintains the conformational stability of the β chain. The C- terminal domain contains several tyrosines and serines, that are phosphorylated and have mitogenic roles, but how they actually contribute to normal and malignant IGF-IR signaling is still not fully understood (35) (**Figure 4**).

Binding of IGF-IR to its ligands causes the phosphorylation of tyrosines on the intracellular portion of its β subunit. Once phosphorylated, tyrosine 950 provides a docking site for its substrates, IRS 1-4 and shc domain protein. Upon substrate binding, downstream signaling is activated through PI3K/Akt , MAPK, or JAK/STAT pathways and may stimulate cancer cell growth in an autocrine/paracrine manner (36, 37) (**Figure 5**).
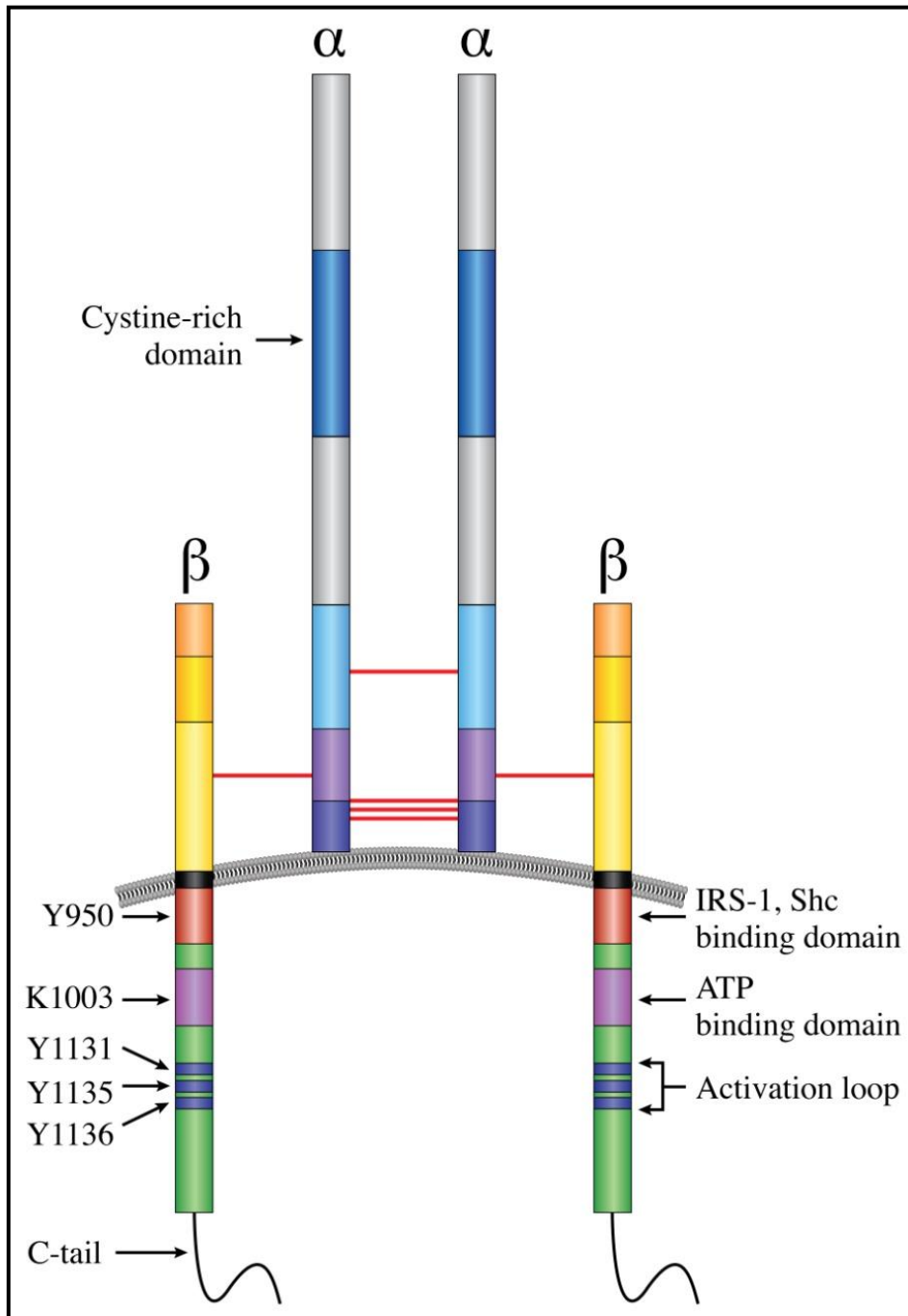
Figure 4: Structure of IGF-IR: IGF-IR is transmembrane homodimeric receptor tyrosine kinase consisting of two identical α subunits and two identical β subunits connected by disulfide bridges. The extracellular α subunit contains a cysteine rich domain where the ligand binds. The cytoplasmic region contains residues involved in the activation of IGF-IR. Y950 is the binding site for its primary substrates, IRS-1 and shc. K1003 is the ATP binding domain. Y1131, 1135, and 1136 make up the activation loop of the kinase domain followed by the C-terminal end.
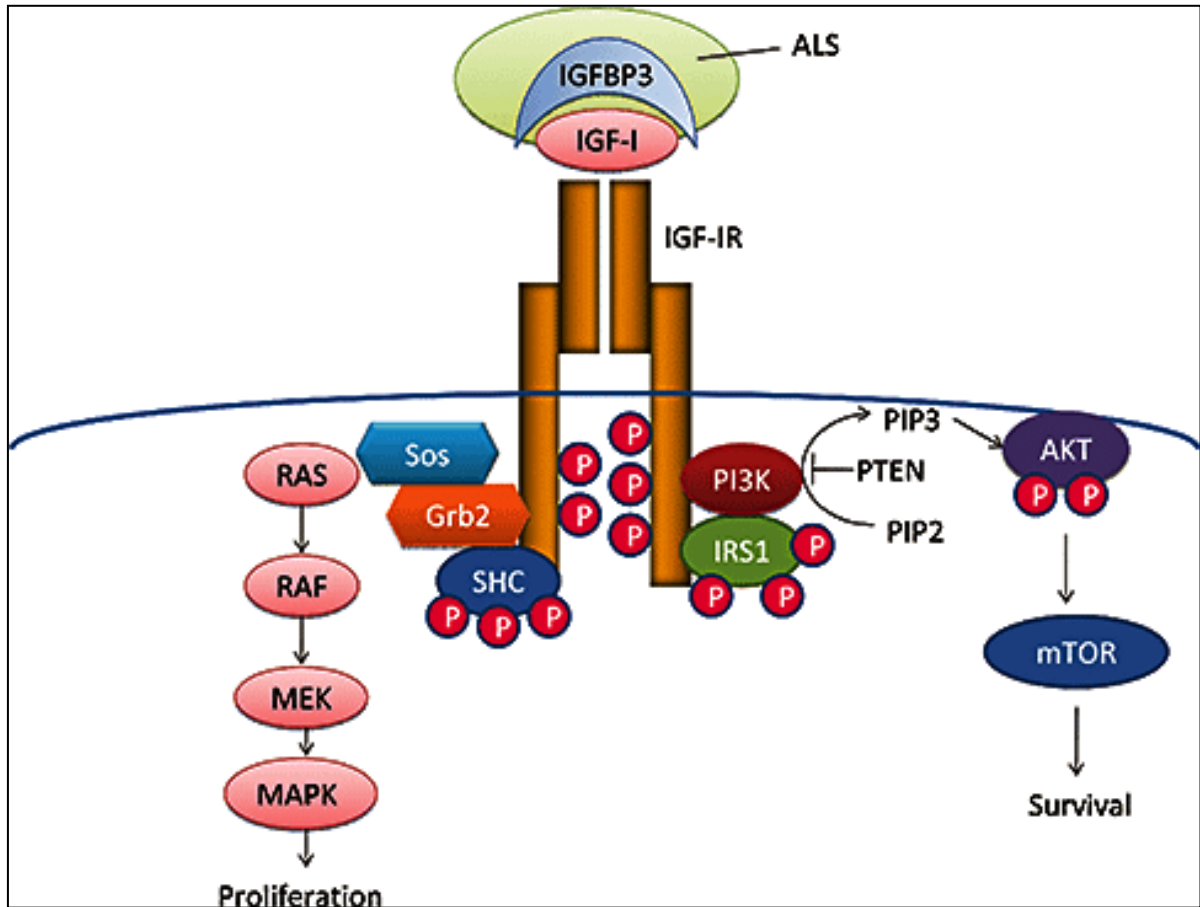
Figure 5: IGF-IR signaling: Binding of IGF-IR to its ligands causes the phosphorylation of tyrosines on the intracellular portion of its β subunit. Once phosphorylated, tyrosine 950 provides a docking site for its substrates, IRS 1-4 and shc domain protein. Upon substrate binding, downstream signaling is activated through PI3K/Akt, MAPK, or JAK/STAT pathways. Adapted from Kojima, S. et al: International Journal of urology Vol. 16, 2009:161-167. Copyright 2008 by JOHN WILEY AND SONS. Reproduced with permission of JOHN WILEY AND SONS in the format Dissertation via Copyright Clearance Center.

1.5 c. Physiological and pathological roles of IGF-IR

Mouse models have confirmed the importance of IGF-IR in prenatal and postnatal growth, especially in regards to genetic imprinting. The result of activation of IGF-IR during these stages is survival and proliferation in mitosis-competent cells resulting in growth of tissues such as skeletal muscle and cardiac muscle (15, 19, 38-41). It also plays a critical role during development of mammary gland tissue during pregnancy and lactation. It has been previously shown that *Igf1r* null mice develop generalized organ hypoplasia, including developmental delays in bone ossification, and abnormalities in the central nervous system (15, 19, 42-45). During embryonic development, the IGF-IR pathway is also involved in the development of limb buds.   Mice lacking the entire *Igf1r* gene die early in development (invariably at birth) due to severe respiratory failure and also exhibit a dramatic reduction in body mass, testifying to the strong growth-promoting effect of this receptor (42). Mice carrying only one functional copy of *Igf1r* are normal, but exhibit a ~45% decrease in body mass (42).

The IGF-IR pathway is also strongly associated with initiating cancer growth (25, 36, 38, 46-57). Evidence in the last 20 years has emerged to support that IGF-IR overexpression plays a significant role in the development and progression of tumors, metastatic potential, and resistance to new therapies. Studies have shown that IGF-IR induces its oncogenic effects through the inhibition of apoptosis and induction of transformation, metastasis, and angiogenesis. Recent studies have claimed that a constitutively active IGF-IR can induce ligand-independent tumor cell progression and more importantly, may be critically necessary in mediating certain oncogenes during their transforming processes. For example, treatment of RM11A cells (murine breast cancer cell line) with high levels of IGF-IR with exogenous IGF-I, IGF-II, or serum did not enhance the proliferative/survival advantage (58). On the other hand, the ability of RM11A cells expressing low levels of IGF-IR to respond to IGF stimulation was found most likely to be due to activation of the

endogenous murine IGF-IR. Therefore, it was concluded that it is possible that IGF-IR

overexpression results in constitutive activation of the IGF-IR independent of the presence

of ligands (58). In addition, autoactivation of IGF-IR, when expressed at sufficient levels,

has previously been shown in cells lacking IGF-IR that have been transfected with different

levels of IGF-IR (59). Furthermore, IGF-IR regulates properties that cause the malignant

cells to overcome anchorage-dependent growth, allowing them to acquire characteristics

involved in enduring detachment and migration that are essential attributes for metastasis

(60).

It has been shown that the number of IGF-IR molecules present in cells plays a key role

in its transforming properties (59, 61). In fibroblasts, IGF-IR number needs to be greater

than 20,000 receptors per cell to enable mitogenesis after stimulation with IGF-I. Similarly,

in a pancreatic cell line model, the observed increase in receptor number from 40,000

receptors/cell to 100,000 receptors/cell is in the range required to enable IGF-I-stimulated

growth and therefore may be of central importance for pancreatic tumor growth control.

Based on these findings, it is concluded that only a small increment in the number of

receptors per cell can induce the transforming properties of IGF-IR in different types of

tumors (59, 61).

In solid tumors, some studies for the role of the IGF system have been performed using

breast cancer cell lines, and was found that one of the mechanisms that IGF-IR was

activated both in vitro and in vivo was through IGF-I: 1) serum IGF-I may act as a

stimulatory molecule to induce the proliferation of breast cancer cells in an endocrine

manner and/or 2) stromal cells that surround the tumorigenic cells serve as a paracrine

stimulator of the mitogenic signal (52, 62-65). It has been shown that there is hindrance of

cell proliferation by cancer cells when IGF-IR activation is inhibited. One possible

mechanism is the lack of interaction of IGFs with IGF-IR or interrupting the signaling

pathway. In prostate cancer, IGFs have been shown to directly stimulate the androgen

receptor (AR) via crosstalk with IGF-IR on prostatic epithelial cells to induce its pathogenesis, progression, and metastisis (66). Similarly, the oncogenic effects of IGF-IR are also seen in colon cancer. IGF-IR is overexpressed in colon cancer, compared to normal colonic mucosa and IGFs in colonic malignant mucosa are shown to exert their effects via the IGF-IR only (27, 56).

In contrast to the widely studied solid tumors, not many studies have been performed to examine the role of IGF-IR in hematological neoplasms and, most of the studies have focused primarily on plasma cell myeloma (67, 68).

1.6 Role of IGF-IR in cell cycle progression and apoptosis

The strong mitogenic properties of IGF-IR are evident through its ability to positively and negatively regulate cell cycle progression and inhibit apoptosis. It has been previously shown that IGF-IR can regulate cell-cycle progression through control of several cell cycle checkpoints. At the G0/G1 phase of the cell cycle, it activates the p70S6K (a kinase that is responsible for site-specific phosphorylation of Bad, which inactivates this pro-apoptotic molecule), leading to phosphorylation of the S6 ribosomal protein and a subsequent increase in the ribosomal pool necessary for entry into the cell cycle (69). However, its most notable contribution to the cell cycle occurs during the G1/S phase transition.

At the G1/S transition, IGF-IR increases synthesis of cyclin E mRNA, which normally complexes with CDK2 to allow for entry from the G1 phase to the S phase of the cell cycle (69). However, the most significant contribution of IGF-IR to this phase of the cell cycle is through the regulation of cyclin D1. IGF-IR increases cyclin D1 and CDK4 gene expression, leading to phosphorylation of Rb1, and release of the E2F transcription factor (69, 70). Cyclin D1 expression can be mediated through several IGF-IR induced mechanisms. For example, it can be transcriptionally regulated through the ras/raf1/MEK/ERK pathway or it may be mediated through increased translation of its mRNA in a PI3K/Akt-dependent manner (71). One study has shown that IGF-IR-axis-induced expression of activated Ras is associated with the increased transcription of cyclin D1 mRNA in IGF-I stimulated human osteocarcinoma cells (72). It was observed that in these cells IGF-IR stimulates the CDKs through Ras activation, and that stimulation is associated with an increase in cyclin D1 mRNA and protein expression, most likely due at least in part to an increase in the rate of transcription initiation of the gene. It was also found that the increase in cyclin D1 most likely occurs in early G1, which corresponds to the portion of the cell cycle in which IGF-IR acts on these cells.

Another study has shown that exongenous addition of IGF-I to a breast cancer cell line activated IGF-IR, with a simultaneous nuclear accumulation of cyclin D1 and activation of the PI3K pathway, but not the MAP/Erk pathway (70) . It was observed that IGF-IR dose-dependently raised cyclin D1 levels in serum-starved cells with exogenous addition of IGF-I. Subsequent activation of the cyclin E/CDK2 complex, hyperphosphorylation of pRb1, and DNA synthesis were detected only in cells treated with mitogenic concentrations of IGF-I. Also, using specific inhibitors, this study showed activation of the PI3K pathway by IGF-IR to be essential for cell cycle progression. The PI3K inhibitor LY294002 completely abolished nuclear accumulation of cyclin D1 protein in late G1 phase, but the MEK inhibitor PD098059 did not significantly block translocation of cyclin D1 to the nucleus, suggesting that the ERK pathway is not critically involved in induction of nuclear accumulation. More importantly, this effect on cyclin D1 was found to be due to an increase in the translation of its mRNA. Therefore, these experiments may suggest that one mechanism of cyclin D1 regulation by IGF-IR is by increasing transcription of cyclin D1 mRNA through the raf/ras/MAPK/Erk pathway or by increasing translation of cyclin D1 mRNA into protein through the PI3K/Akt pathway.

Another mechanism of cyclin D1 upregulation is by downregulating the transcription of the CDK inhibitor p27 by altering its processing and nuclear localization through a PTEN-dependent mechanism (73). A study analyzing the effects of loss of both p21and p27 in mouse embryo fibroblasts after IGF-I treatment demonstrated not only an increase of cyclin D/CDK activity but also markedly increased cyclin D1 protein levels. The loss of p27 resulted in its translocation to the nucleus through the downregulation of PTEN, which normally functions to dephosphorylate PIP3 (thereby rendering it inactive), an activator of the PI3K/Akt pathway. Therefore, this effect induced cell cycle progression from the G1 to the S phase of the cell cycle.

Finally, at the G2/M phase of the cell cycle, IGF-IR increases the mRNA expression of cyclin A and B and Cdc2 synthesis (69). Thus, IGF-IR can positively regulate cell cycle progression at several phases.

IGF-IR has previously been shown to inhibit apoptosis by inhibiting release of cytochrome C through the activation of the PI3K/Akt pathway. Activated Akt can phosphorylate the pro-apoptotic protein Bad. Upon phosphorylation, Bad is dissociated from anti-apoptotic Bcl-2, and becomes temporarily controlled by the adaptor protein 14-3-3. If Bad is not phosphorylated, other pro-apoptotic proteins, such as Bak and Bax, become activated and cause cytochrome C release from mitochondria. In turn, caspase-9 and then caspase-3 become activated. Activated caspase-3 can cleave and inactivate, for example, the poly(ADP-ribose) polymerase (PARP), which normally functions in DNA repair and programmed cell death and this results in extensive degradation of DNA at the final steps in the apoptotic process (74, 75).
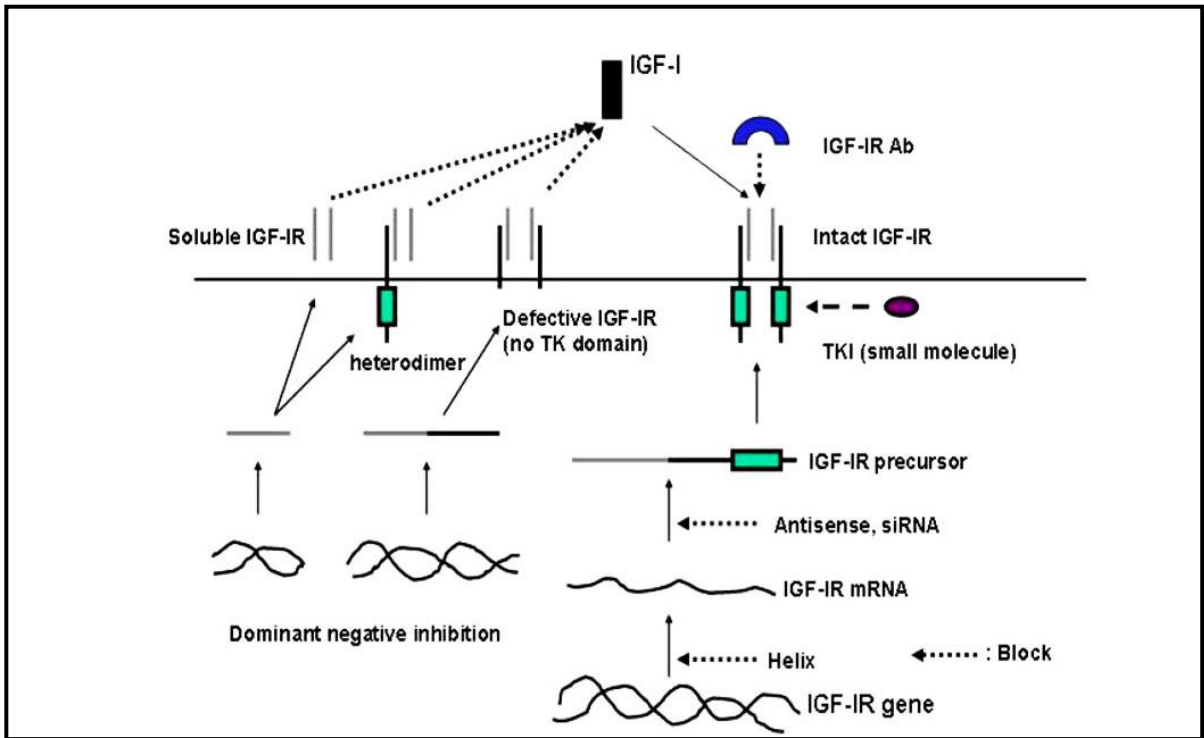
1.7 Current approaches to target IGF-IR

Currently there are several approaches to target IGF-IR including antisense plasmids, dominant negative strategies, and siRNA (50, 76-82) (**Figure 6**). However, the most notable approaches have been the recent development of anti-IGF-IR antibodies and small molecule inhibitors of IGF-IR. Recently, at least 8 human monoclonal antibodies have been tested in clinical trials (83). However, using monoclonal antibodies as treatment has induced hyperglycemia in some patients, as these antibodies can also target the insulin receptor (83). Therefore, a need for developing more specific approaches to targeting IGF-IR is the focus of many studies. IGF-IR and IR are both tyrosine kinases with identical ATP binding sites, therefore, the best approach for designing small molecule inhibitors is to target receptor autophosphorylation at the substrate level. An example of such small molecule inhibitors includes the family of cyclolignans (84). These have been shown to mimic the three dimensional structure of the IGF-IR tyrosine kinase domain, preventing substrate binding, and inducing apoptosis and cell cycle arrest in several solid tumors (84-88).

One particular member of the cyclolignan family is picropodophyllin (PPP). PPP has been shown to be an activation-loop small molecule inhibitor of IGF-IR and currently is in pre-clinical development (84, 89, 90). In a very recent study, PPP was found to be the most efficient compared to other antitumor agents (imatinib mesylate and 3 other cytostatic agents) in killing uveal melanoma cells after oral administration in a SCID mouse model (91). PPP was well tolerated by the animals and also decreased VEGF expression in the tumors. It was demonstrated previously that PPP is an inhibitor of the IGF-IR tyrosine phosphorylation and importantly that it did not interfere with the highly homologous insulin receptor (IR) (84, 90). PPP did not selectively inhibit the IGF-IR tyrosine kinase at the level of ATP binding, since the ATP domain is structurally similar to the one found in the IR. This suggests that it acted through suppression of other components, such as at the level of

receptor substrate. Normally, IGF-IR, in its inactive state, contains the activation loop which

houses the critical tyrosine residues 1131, 1135, and 1136. Y1135 (being the first tyrosine

to be phosphorylated) in the activation loop is bound in a *cis* position and therefore prevents

any access by the substrates or ATP. After ligand binding, the three tyrosines of the

activation loop are phosphorylated to a *trans* position in the β subunit.   Phosphorylation of

Y1135 and Y1131 destabilizes the autoinhibitory conformation of the activation loop, while

phosphorylation of Y1136 residue stabilizes the active conformation of IGF-IR (92). These

changes in the activation loop conformation allow for substrate and ATP binding and

subsequent activation of downstream signaling of IGF-IR.   PPP is said to selectively inhibit

phosphorylation of Y1136 of the activation loop while refraining from Y1131 and Y1135,

thereby preventing the stabilization of IGF-IR. This approach is considered more selective

and less cytotoxic, therefore, targeting the IGF signaling pathway with small molecule

inhibitors such as PPP represents a promising strategy in the development of novel anti-

cancer therapeutics.

Figure 6: Current approaches to target IGF-IR. Adapted from Lee, T. et al: Gene Ther Mol Biol Vol.9, 2005: 77-88

Rationale

   The rationale behind our study is that:

1) MCL is an aggressive, incurable type of malignant lymphoma that currently has no target-based therapeutic approach. As previously mentioned, current treatments for MCL include chemotherapy combinations plus rituximab such as R-CHOP and more aggressive treatments such as R-HyperCVAD. Other approaches include radioimmunotherapy combinations with rituximab, proteosome inhibitors such as Velcade, and stem cell transplantations. Although these treatments prove to be initially effective, the patient almost always develops resistance/relapse due to the highly aggressive nature of the disease. Therefore, targeting specific signaling pathways deregulated in MCL, particularly those regulating cell proliferation and cell death is opening new doors for therapeutic intervention.

2) IGF-IR appears to be a promising molecular target in aggressive solid tumors and is currently being tested in clinical trials. As a drug target, the IGF system has a number of key features that proves itself to being appealing. The expression of IGF-IR, the major signal transducing receptor of the pathway, appears to be necessary for malignant transformation in preclinical models. IGF-IR overexpression has been well documented in a number of aggressive solid tumors. Several IGF-IR inhibitors are in the clinical or pre-clinical stages of development, including a member of the cyclolignan family of inhibitors called picropodophyllin, PPP.

3) Overlap exists between pathogenetic molecular mechanisms in MCL and IGF-IR signaling system. The main signaling pathways involved in both the pathogenesis of MCL as well as IGF-IR signaling include PI3K/Akt, MAPK, and JAK/STAT pathways. More specifically, both MCL and IGF-IR signaling systems regulate common key molecules that are involved in cell cycle progression and apoptosis in which the three main signaling systems contribute. For example, MCL is characterized by the genetic translocation

t(11;14)(q13;q32) resulting in the overproduction of cyclin D1, a cell cycle regulatory molecule that functions at the G1/S transition phase. Recent studies have shown that cyclin D1 may be mediated through increased translation in a PI3K/Akt-dependent manner or it can be transcriptionally regulated through the ERK pathway by IGF-IR. In addition, common pro-apoptotic molecules and anti-apoptotic molecules have been shown to be deregulated in both systems. Therefore, targeting IGF-IR may possibily induce cell cycle arrest and apoptosis through these shared molecules in MCL cells.

We hypothesize that IGF-IR signaling contributes to the survival of MCL and thus may prove to be a legitimate therapeutic target in the future. In order to test our hypothesis, we proposed the following set of aims:

Aim 1: To analyze the expression of IGF-IR and its activation in MCL.

Aim 2: To test the effects of inhibition of IGF-IR in MCL.

Chapter II: Analysis of the Expression of IGF-IR and Its Activation in Mantle Cell Lymphoma

2.1 IGF-IR expression in MCL

To examine the expression of IGF-IR mRNA in MCL, 4 established MCL cell lines (SP-53, JeKo-1, Mino, and Granta) were used to perform RT- PCR using IGF-IRα and IGF-IRβ primers. Normal human peripheral blood CD19$^+$ B-lymphocytes were used to analyze the physiological level of expression of IGF-IR. Karpas 299 and P6 cell lines were used as positive controls. The R- cell line was used as a negative control. As shown in **Figure 7**, all MCL cell lines showed overexpression of IGF-IRα as well as IGF-IRβ mRNA compared to normal B-lymphocytes. SP-53 and Granta displayed lower levels of expression relative to JeKo-1 and Mino. Karpas 299 and P6 expressed IGF-IRα and IGF-IRβ, whereas R- was completely negative for IGF-IRα, but displayed a very low level of expression of the IGF-IRβ subunit.
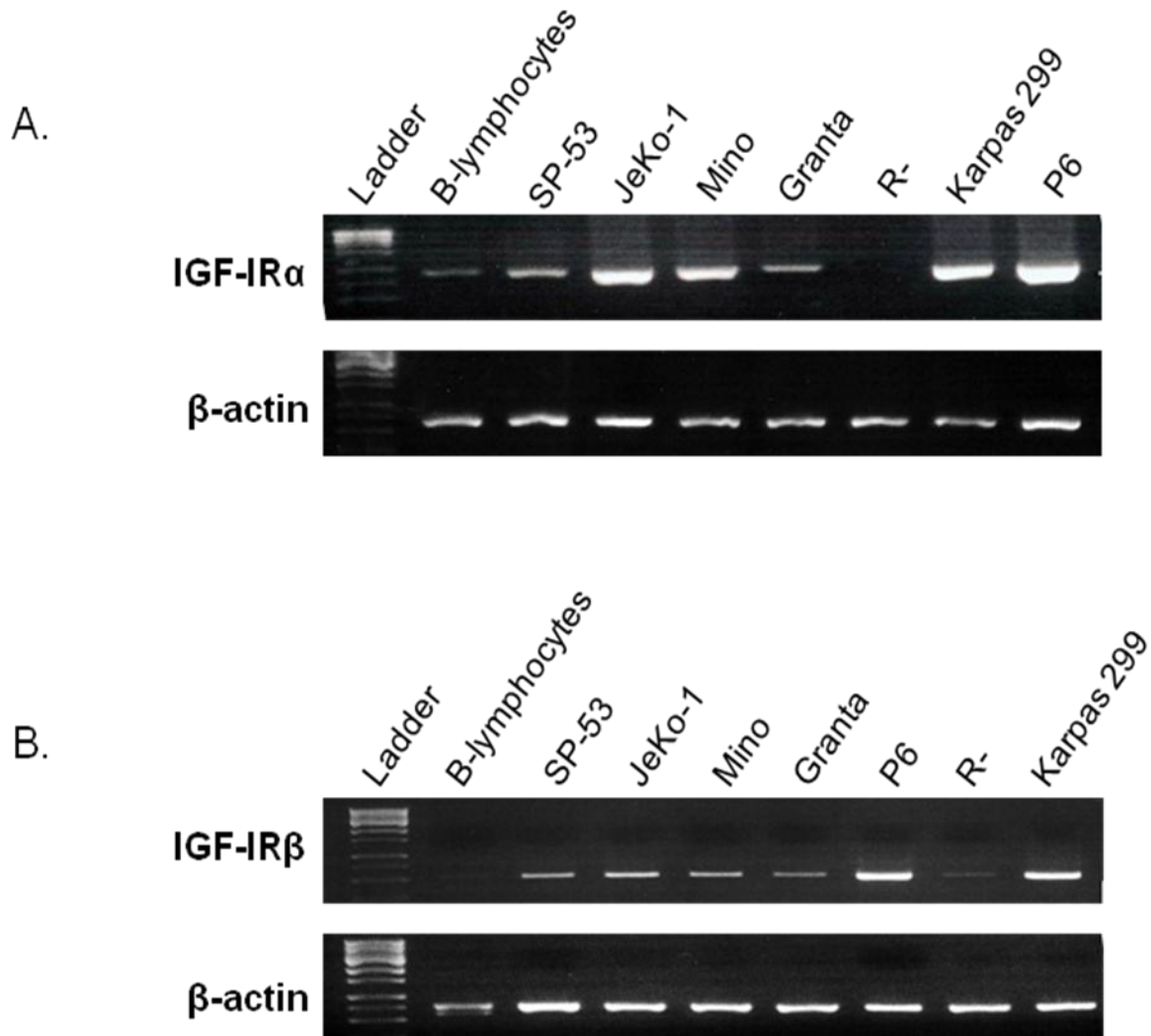
Figure 7. Expression of IGF-IR mRNA in MCL: (A) RT-PCR demonstrates the expression of IGF-IRα mRNA in 4 MCL cell lines (SP-53, JeKo-1, Mino, and Granta) relative to normal peripheral blood CD19+ B-lymphocytes. The cell lines Karpas 299 and P6 were used as positive controls. The cell line R- was used as a negative control. **(B)** RT-PCR showing IGF-IRβ expression. Overexpression was observed in MCL cell lines relative to normal peripheral blood CD19+ B-lymphocytes. Karpas 299 and P6 expressed both IGF-IRα and IGF-IRβ. A very low level IGF-IRβ was detected in R- cells and B-lymphocytes.

To explore the expression of IGF-IR protein in MCL, 3 MCL cell lines (SP-53, JeKo-1, and Mino) were used to perform Western blotting using an anti- IGFIRβ antibody. Consistent with the results of mRNA expression levels, SP-53 showed lower levels of IGF-IRβ, whereas JeKo-1 and Mino showed a higher level of expression. The control cell lines Karpas 299 and R- demonstrated positive and negative expression for IGF-IR protein, respectively **(Figure 8)**. RSC96 (Schwann cell line) was used as an additional negative control.
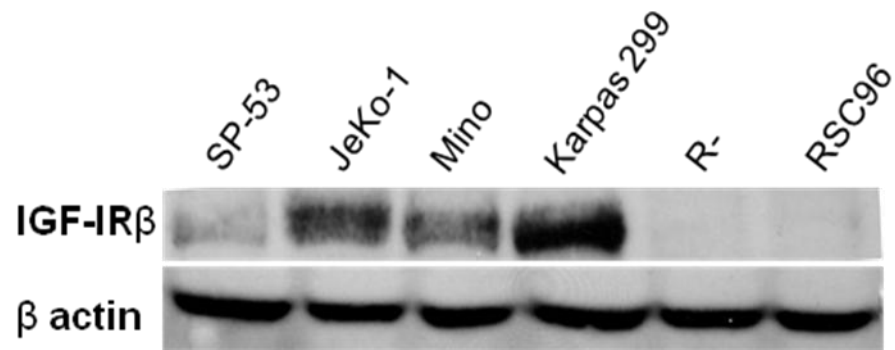
Figure 8. Expression of IGF-IR protein in MCL: Western blotting demonstrates the expression of IGF-IRβ protein in 3 MCL cell lines (SP-53, JeKo-1, and Mino). The cell lines R- and RSC96 were used as negative controls and Karpas 299 was used as a positive control. SP-53 showed lower level of expression of IGF-IRβ compared with JeKo-1 and Mino.

To demonstrate the localization of IGF-IR in MCL cells, we performed immunohistochemical and immunofluorescence staining of 3 MCL cell lines and Karpas 299 (positive control) and R- (negative control). As shown in **Figure 9**, all 3 cell lines and the positive control showed significant expression of IGF-IR protein in the membrane and cytoplasm of the cells, whereas R- was completely negative for the receptor.
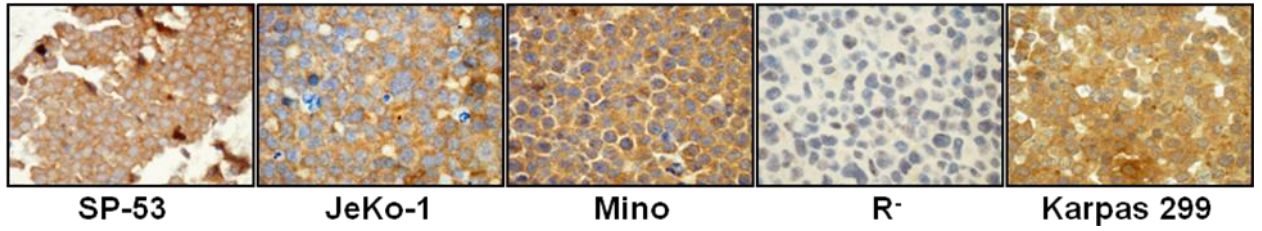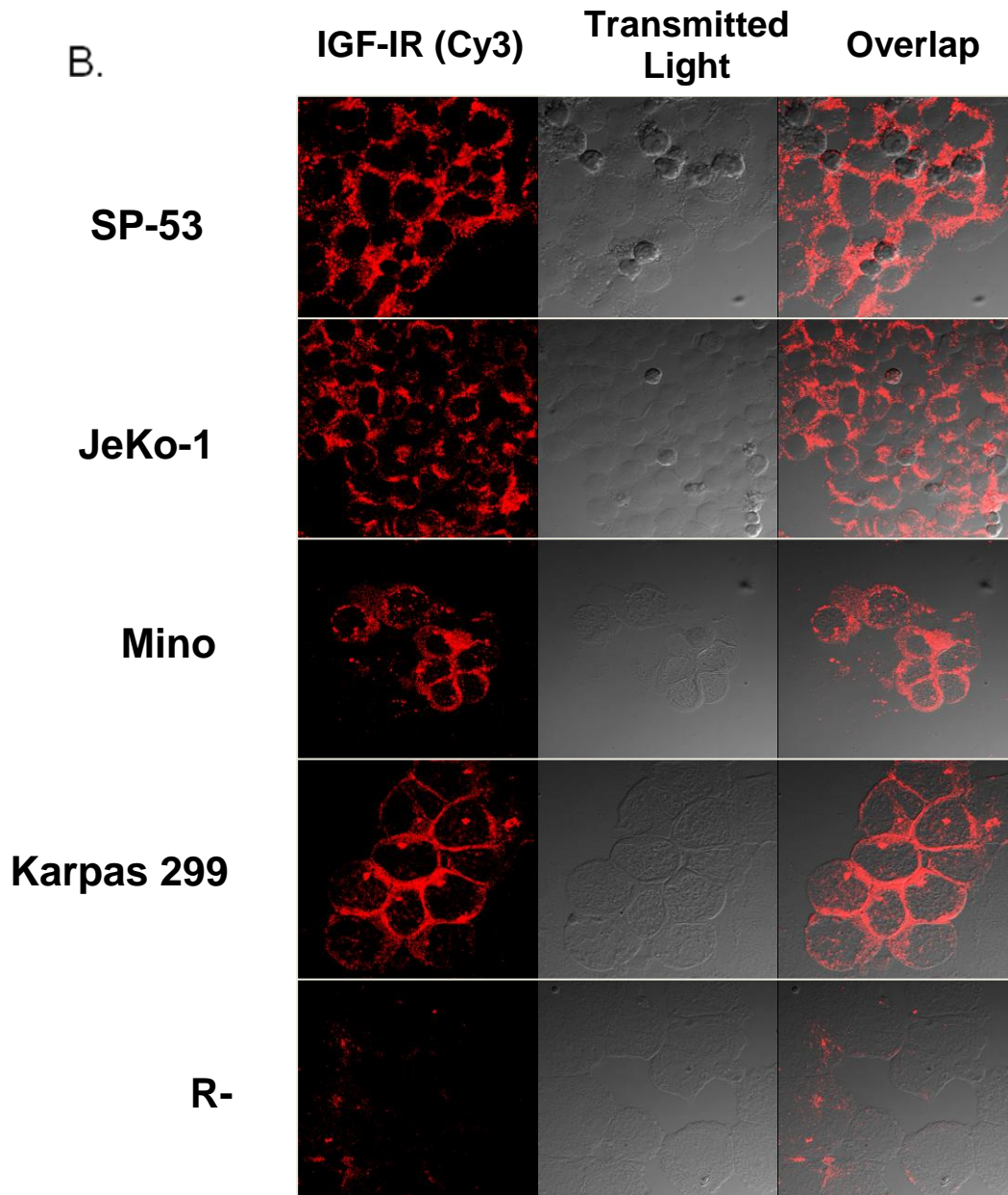
Figure 9. Expression of IGF-IRβ protein in MCL: (A) Immunohistochemical staining revealed IGF-IRβ to be expressed in the cell membrane and cytoplasm. Karpas 299 and R- were used as positive and negative controls, respectively. **(B)** Immunofluorescence showed IGF-IRβ to be expressed in the cell membrane and cytoplasm. Karpas 299 and R- were used as positive and negative controls, respectively.

To evaluate IGF-IR expression levels in MCL, quantitative analysis using flow cytometry was used to measure the relative IGF-IR antigen density per cell. Three MCL cell lines (SP-53, JeKo-1, and Mino) and Karpas 299, R-, and normal B-lymphocytes were incubated with either PE-labeled mouse IgG isotope (blue areas) or PE-labeled IGF-IRα antibody (green peak) and mean fluorescence values were calculated. **Figure 10** shows that all MCL cell lines demonstrated high expression levels compared to normal B-lymphocytes and the negative control R-, after assessing number of IGF-IR molecules/cell considering that the PE:mAb ratio was 1:1. Relative to B-lymphocytes, IGF-IR antigen density per cell was 135-fold, 205-fold, and 420-fold higher in SP-53, JeKo-1, and Mino, respectively.

SP-53

2.7 x10^4

JeKo-1

4.1 x10^4

Mino

8.4 x10^4

Karpas 299

12.0 x10^4

R-

No expression

B-Lymphocytes

0.02 x10^4
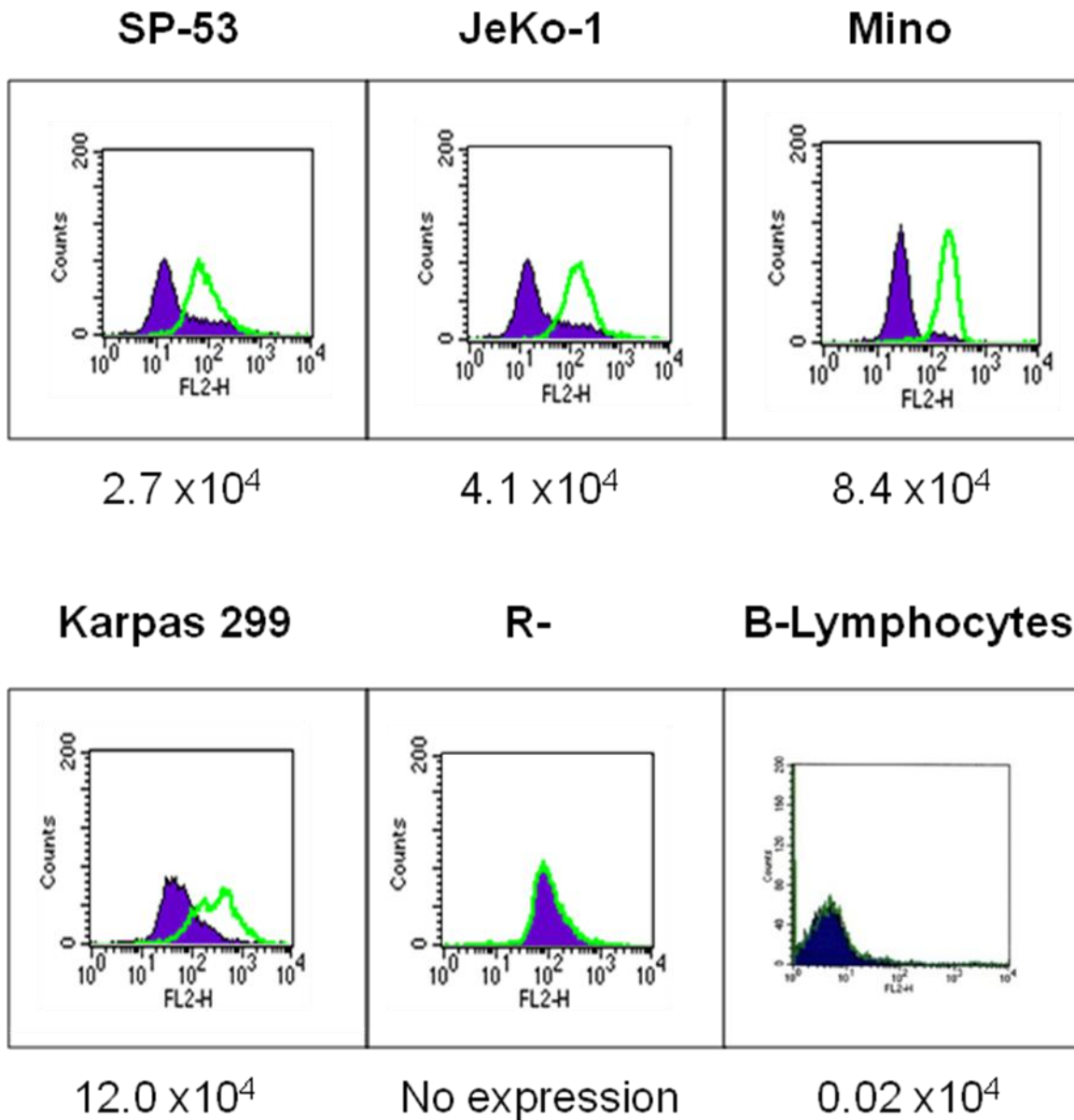
Figure 10. Quantitative analysis of IGF-IR expression: Flow cytometry analyzing relative IGF-IR antigen density per cell was consistent with the results of WB. MCL cells and control cell lines Karpas 299, R-, and normal B- lymphocytes were incubated with either mouse IgG isotope (blue areas) or IGF-IRα antibody (green peak). Compared with normal B-lymphocytes and the negative control cell line R-, the 3 MCL cell lines displayed high levels of IGF-IRα, as observed in a shift in peaks based on mean fluorescence absorbance. IGF-IRα molecules/cell is shown in this figure.

Because we found the expression of IGF-IR in SP-53, JeKo-1, and Mino, we sought to determine whether the activated/phosphorylated form of IGF-IR (pIGF-IR) is present in these cells. In order to do so, immunoprecipitation and Western blotting techniques were used. IGF-IRβ was immunoprecipitated using an anti-IGF-IRβ antibody by adding total protein extracts (800 μg) to agarose beads conjugated with A/G. Proteins were then subjected to Western blotting and subsequently stained with anti-p-Tyr antibody or IGF-IR antibody **(Figure 11).** pIGF-IR was expressed in MCL cells. SP-53 showed lower level of phosphorylation relative to JeKo-1 and Mino. Beads only was used as a reagent control. Cell lysate immunoprecipitated with mouse IgG was used to distinguish IGF-IRβ protein from nonspecific bands.
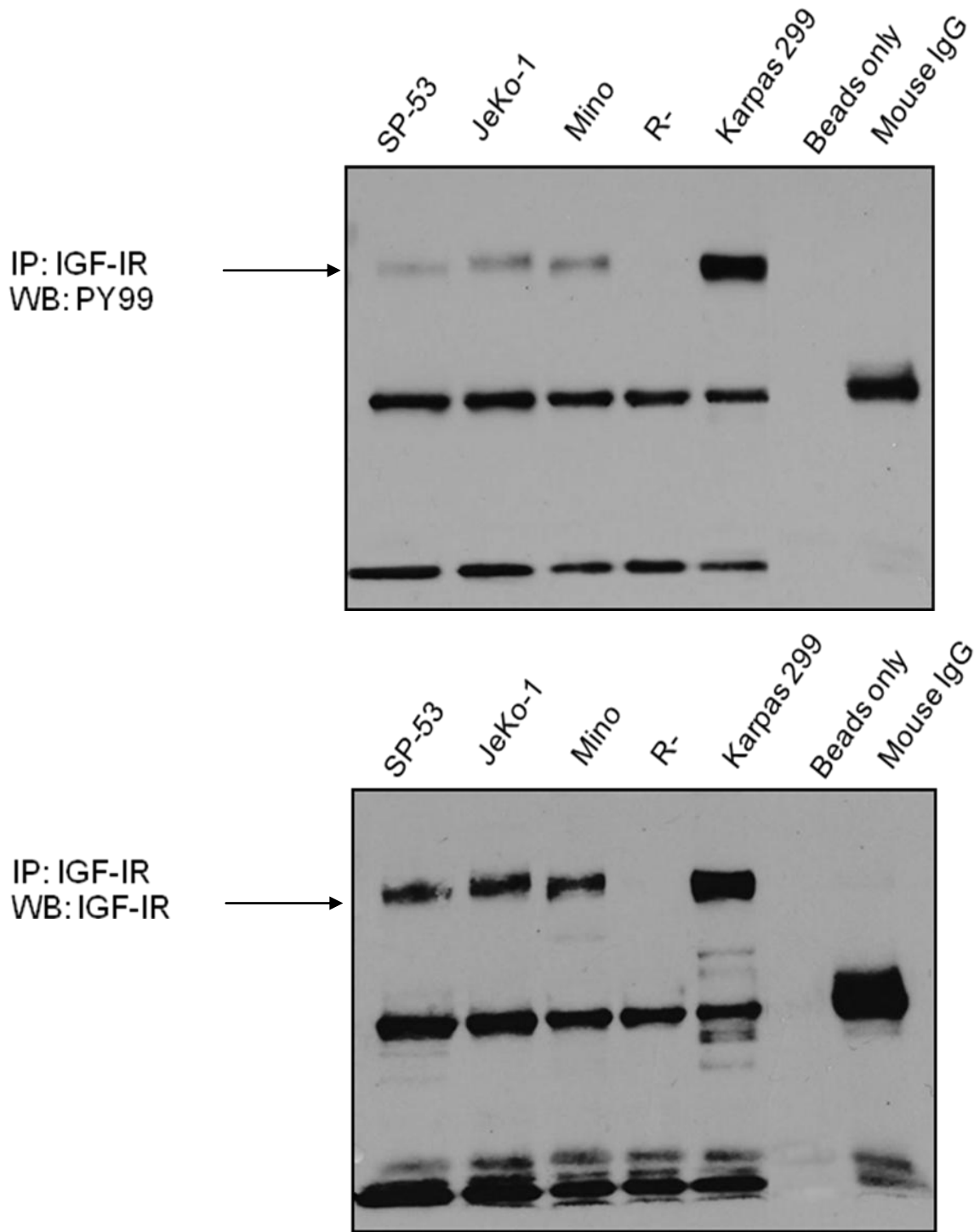
Figure 11. Expression of pIGF-IR in MCL: Cell lysates from SP-53, JeKo-1, Mino and control cell lines were immunoprecipitated with IGF-IRβ antibody and then subsequently stained with either pY99 antibody or IGF-IRβ antibody. Immunoprecipitation revealed that all 3 MCL cell lines were phosphorylated at varying levels. Karpas 299 and R- cell lines were used as positive and negative controls respectively. Beads only were used as a reagent control. Cell lysate immunoprecipitated with mouse IgG was used to distinguish IGF-IRβ protein from nonspecific bands.

2.2 IGF-I expression in MCL

IGF-I is the primary ligand of IGF-IR. Therefore, we tested the expression of IGF-I in 3 MCL cell lines. RT-PCR was performed using 2 different sets of primers to confirm the results. As shown in **Figure 12**, compared to the positive control, K562 (a chronic myeloid leukemia cell line), we found no apparent expression of IGF-I. RSC96, Karpas 299, and R-cell line were also included as negative controls because these cells lack IGF-I mRNA expression.

To further confirm this result, quantitative real-time PCR was performed using 18s ribosomal RNA as the endogenous control. Any amplification after 35 cycles was considered as no expression. As shown in **Figure 13**, we found negligible amount of IGF-I mRNA expression in SP-53 and no expression of IGF-I mRNA in JeKo-1 and Mino. These findings strongly suggest that IGF-IR is not activated through an autocrine release of IGF-I. K562 and RSC96 were used as positive and negative controls, respectively.
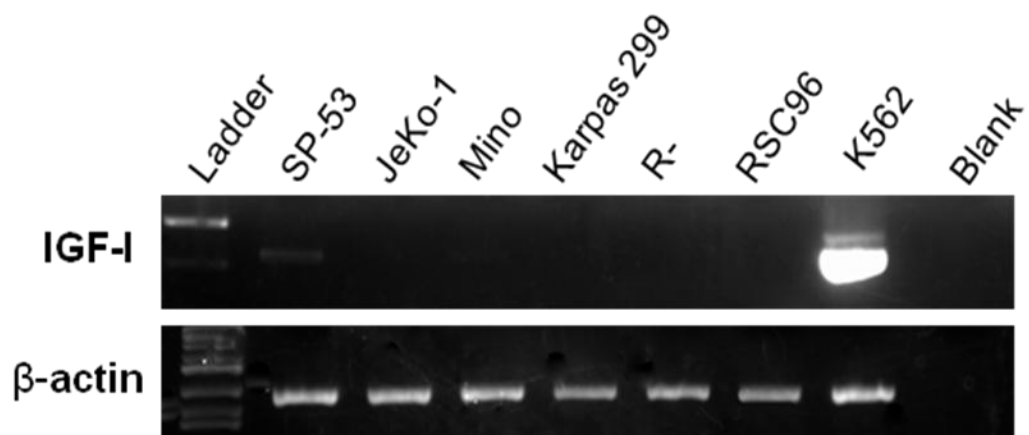
Figure 12. Expression of IGF-I mRNA in MCL cell lines: RT-PCR revealed negligible amount of IGF-I in SP-53 and no apparent expression of IGF-I in JeKo-1 and Mino. Karpas 299, R-, and RSC96 were used as negative controls. K562 was used as a positive control.

Delta Rn vs Cycle
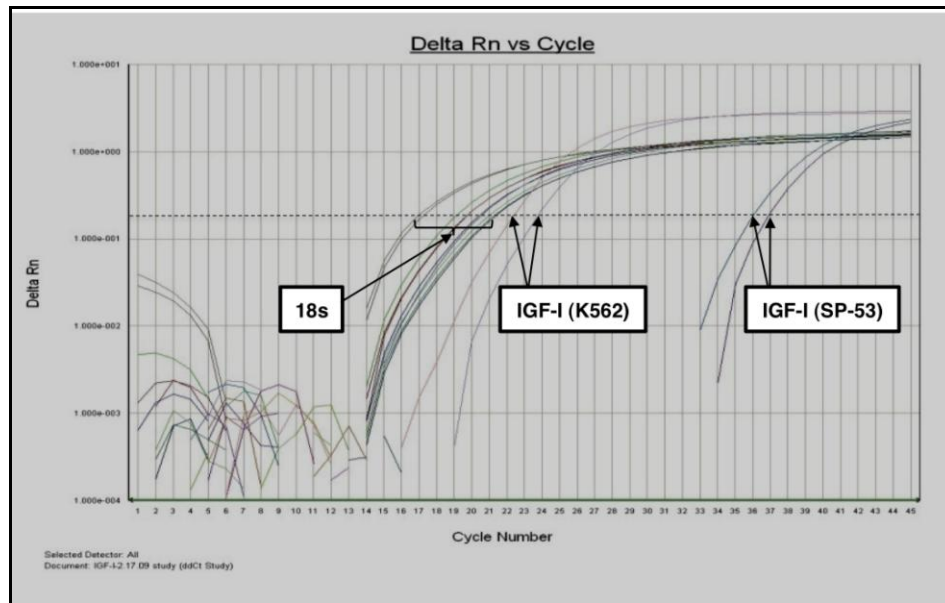
18s			
Sample	**Count 1**	**Count 2**	**Average Count**
SP-53	19.916	19.272	19.594
JeKo-1	20.589	19.91	20.2495
Mino	21.466	21.55	21.508
RSC96	21.186	20.692	20.939
K562	17.397	17.153	17.275
Blank	Undetermined	Undetermined	

IGF-I			
Sample	**Count 1**	**Count 2**	**Average Count**
SP-53	36.112	36.993	36.5525
JeKo-1	Undetermined	Undetermined	
Mino	Undetermined	Undetermined	
RSC96	Undetermined	Undetermined	
K562	23.858	22.42	23.139
Blank	Undetermined	Undetermined	

Figure 13. Expression of IGF-I mRNA in MCL cell lines: To further evaluate the expression of IGF-I mRNA in SP-53, JeKo-1, and Mino, quantitative real-time PCR was performed using 18s ribosomal RNA as the endogenous control. K562 and RSC96 were used as the positive and negative controls, respectively. Experiments were performed in duplicates and averaged. Amplification plot shown represents amount of fluorescence (Rn) measured at each thermal cycle, and is proportional to amount of PCR product generated at that point. Relative quantitation is expressed in terms of cycle threshold (Ct), the cycle at which fluorescence crosses a threshold value. Amplification after 35 cycles was considered as no expression. All cell lines exhibited high expression of 18S ribosomal RNA ranging from 17.275 (most abundant) cycles to 21.508 (least abundant). We found possible negligible amount of IGF-I mRNA expression in SP-53 (36.5525 cycles) and no expression of IGF-I mRNA in JeKo-1 and Mino (undetermined). K562 showed high expression of IGF-I (23.139 cycles) and RSC96 showed no expression (undetermined).

39

In order to test whether IGF-IR signaling axis is functional in MCL, we tested the response of MCL cell lines to IGF-I. To eliminate effects of IGF-I present in FBS, cells were serum-starved MCL cells and were simultaneously treated with IGF-I (500 ng/mL) for 24 hours (SP-53) or 36 hours (Mino) and apoptosis was analyzed using annexin-V/FITC and PI labeling. Cells were considered apoptotic if they were Annexin-V+ only or Annexin-V/FITC+/PI+. Results show that IGF-I decreases apoptosis in MCL cells in a concentration dependent manner. These effects were reversed upon treatment with anti-IGF-IR blocking antibody (5 μg/mL) **(Figure 14).** Untreated starved and unstarved cells (control) were used as controls.
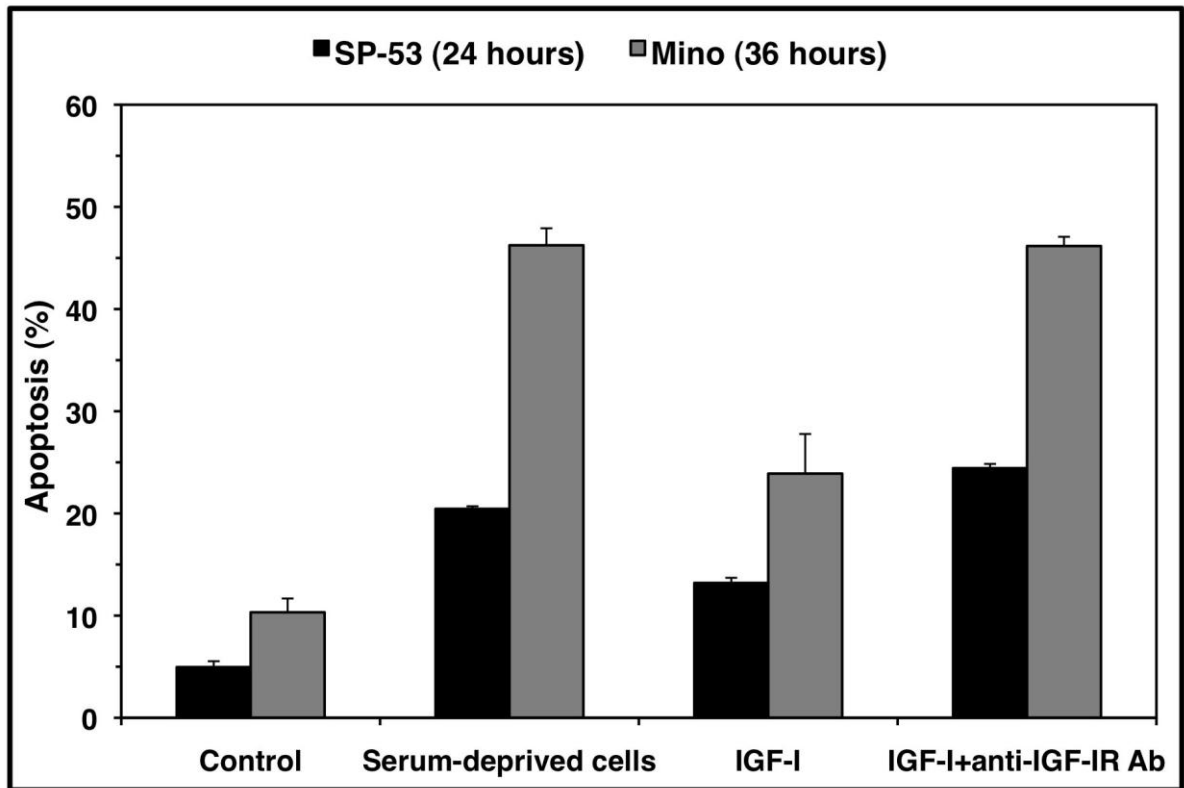
Figure 14. Apoptosis analysis after treatment with IGF-I: MCL cell lines were starved to exclude any effect of IGF-I present in FBS. MCL cells were treated with IGF-I (500 ng/mL) alone or with an IGF-IR blocking antibody (5 μg/mL) for 24 hours (SP-53) or 36 hours (JeKo-1 and Mino) and apoptosis was measured using Annexin-V/FITC and PI labeling. MCL cells showed decrease in apoptosis. Effects of IGF-I on MCL cells were reversed when treated with IGF-IR blocking antibody. Untreated starved and unstarved cells (control) were used as controls. Results are shown as means ± SD.

Chapter III: Effects of inhibition of IGF-IR in

MCL

3.1 Inhibition of IGF-IR by PPP in MCL

To test whether IGF-IR is important for the survival of MCL cells, PPP, a selective inhibitor of IGF-IR, was used. MCL cell line Mino was treated with 4 different concentrations of PPP for 24 hours and 48 hours. Protein lysates were collected and analyzed by Western blotting. PPP downregulated pIGF-IR in a concentration-dependent manner at both time points without altering baseline IGF-IR expression levels and Mino is shown as an example (**Figure 15**). Furthermore, tyrosine kinase activity also decreased in SP-53, JeKo-1, and Mino in a concentration-dependent manner (**Figure 16**).
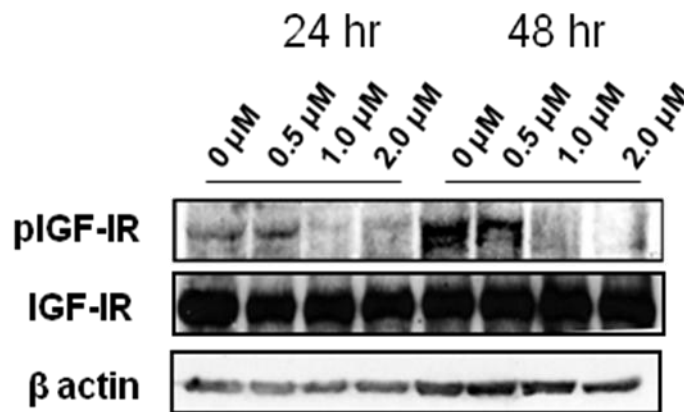
Figure 15. PPP downregulated the activated form of IGF-IR (pIGF-IR) in a concentration-dependent manner at both 24 hours and 48 hours without altering baseline IGF-IR expression levels in Mino cells.
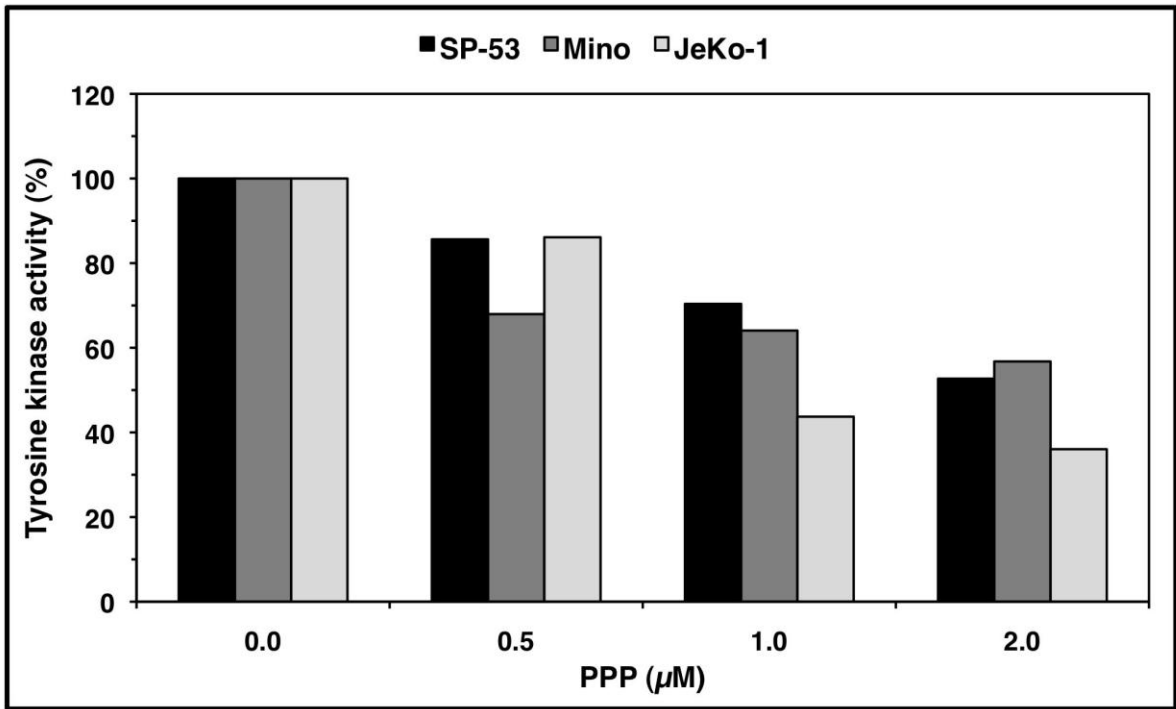
Figure 16. PPP downregulated IGF-IR tyrosine kinase activity in a concentration-dependent manner in SP-53, JeKo-1, and Mino cell lines. Results are the means of one of two consistent experiments.

3.2 Effects of inhibition of IGF-IR by PPP

Cells were treated with PPP using a concentration range of 0.2 to 2.0 µM for 24 or 48 hours. The human skin fibroblast cell line AG01523, which was previously shown to be resistant to PPP (93), and normal B-lymphocytes were both used as negative controls. At 24 hours after PPP treatment, cell viability was assessed using exclusion of staining by trypan blue dye. There was a significant decrease in cell viability in all 3 cell lines. SP-53, JeKo-1, and Mino showed a decrease in cell viability of 20%, 32% and 44%, respectively, at 2 µM (**Figure 17A**). In addition, at 48 hours, all 3 cell lines showed further decrease in viability in a concentration-dependent manner. SP-53, JeKo-1, and Mino showed a decrease of 60%, 62% and 70%, respectively, at 2 µM (**Figure 17B**). The IC_{50} values were 1.0 µM, 1.5 µM, and 1.5 µM for Mino, JeKo-1, and SP-53, respectively.

Induction of apoptosis was also demonstrated by flow cytometry using Annexin-V and PI staining. Cells were considered apoptotic when stained for annexin-V only or when stained simultaneously for annexin-V and PI **(Figure 18).** At 24 hours, SP-53, JeKo-1, and Mino showed increase in apoptosis by 1.7-fold, 3.5-fold, and 3.0-fold relative to untreated cells,respectively. At 48 hours of treatment, SP-53, JeKo-1, and Mino showed increase of 3-fold, 5.5-fold, and 6.3-fold, respectively. Cell cycle analysis using flow cytometry revealed that PPP induces a G2/M cell cycle arrest in all 3 cell lines at 24 hours of treatment **(Figure 19).**

Furthermore, morphological changes associated with apoptosis and cell cycle arrest were demonstrated after staining cytospin slides with Geimsa. Morphological changes associated with apoptosis included nuclear fragmentation and condensation and cell shrinkage (black arrowheads) compared to control untreated cells. Consistent with the G2/M-phase cell cycle arrest, atypical mitotic figures were seen (red arrowheads) **(Figure 20).**

Cell proliferation was assessed using an MTS assay after PPP treatment for both 24 and 48 hours. After 24 hours, cell proliferation was significantly decreased by 66%, 37%, and 54% for SP-53, JeKo-1, and Mino, respectively (**Figure 21A**). After 48 hours of treatment, cell proliferation decreased further to 76%, 52%, and 62% of the control level, for SP-53, JeKo-1, and Mino, respectively **(Figure 21B).**
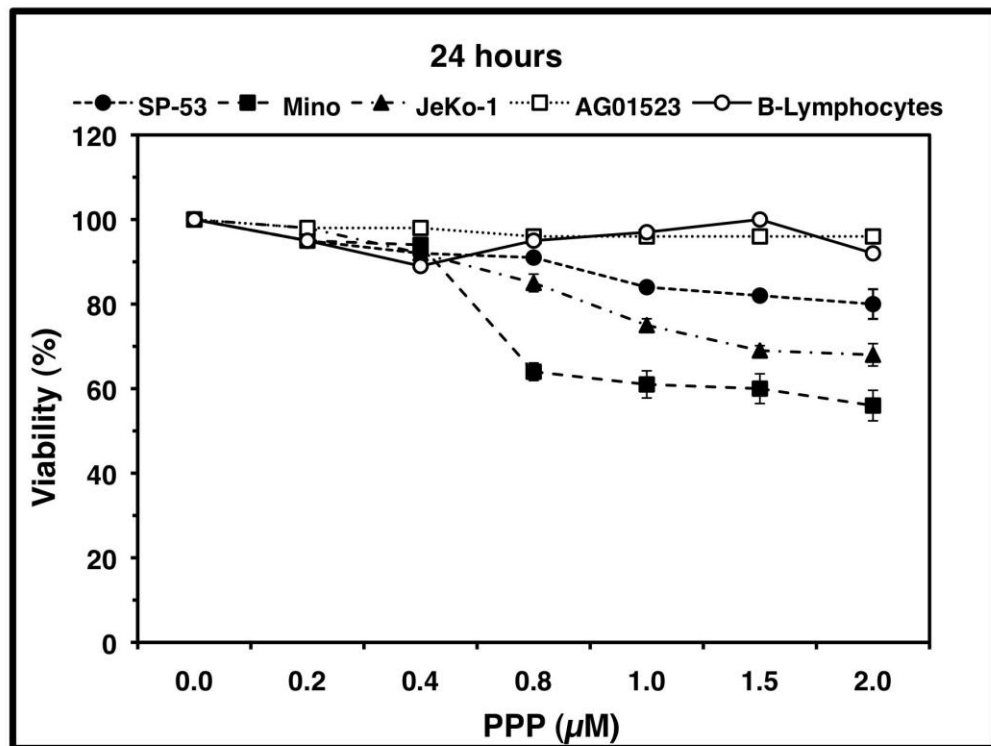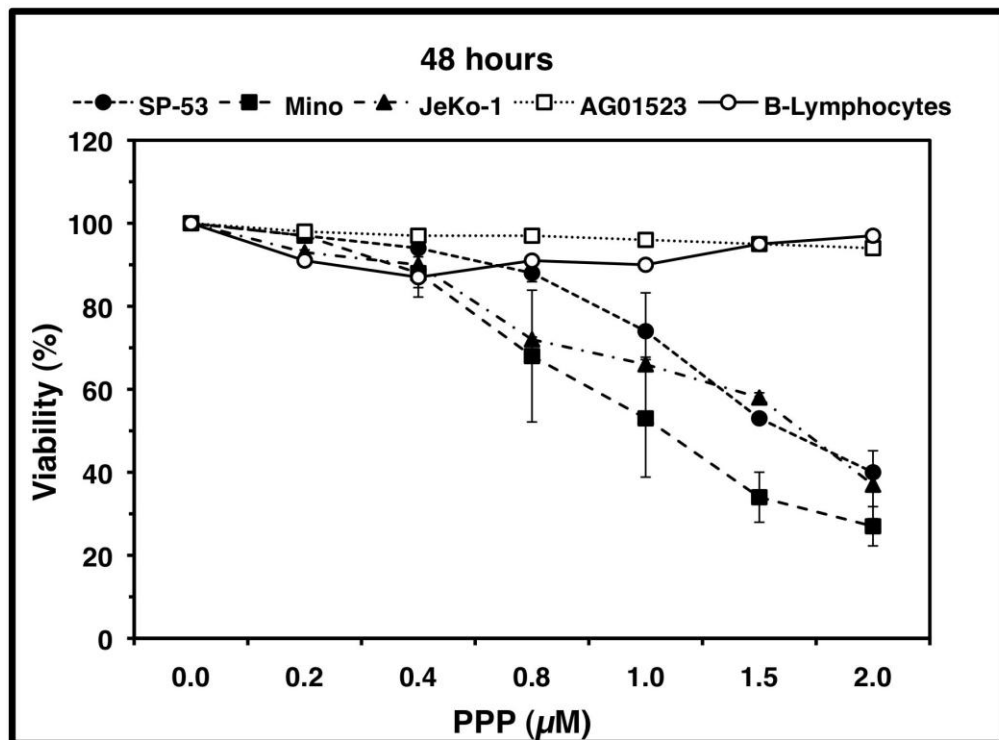
Figure 17. Cell viability after treatment with PPP: (A) MCL cells were treated with PPP using a concentration range of 0.2 to 2.0 µM for 24 hours. Cell viability was determined using exclusion of staining by trypan blue dye and showed decrease in cell viability in a concentration-dependent manner. **(B)** Cell viability decreased further after 48 hours of treatment.
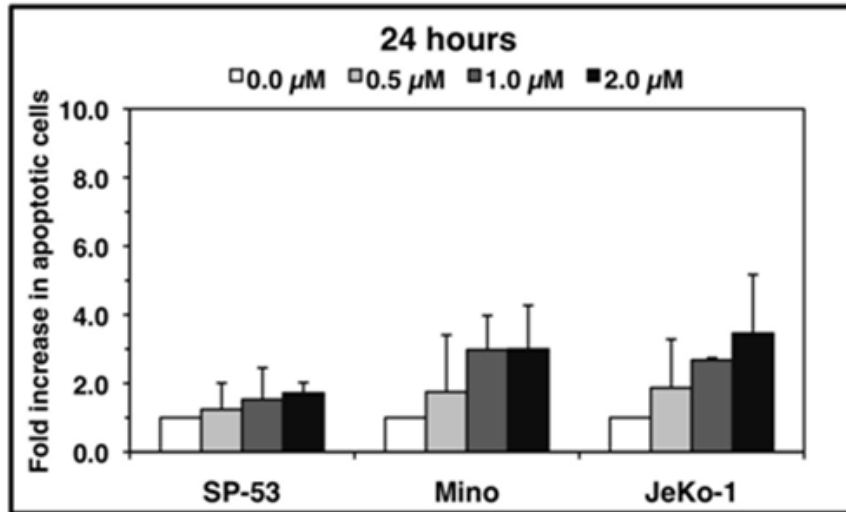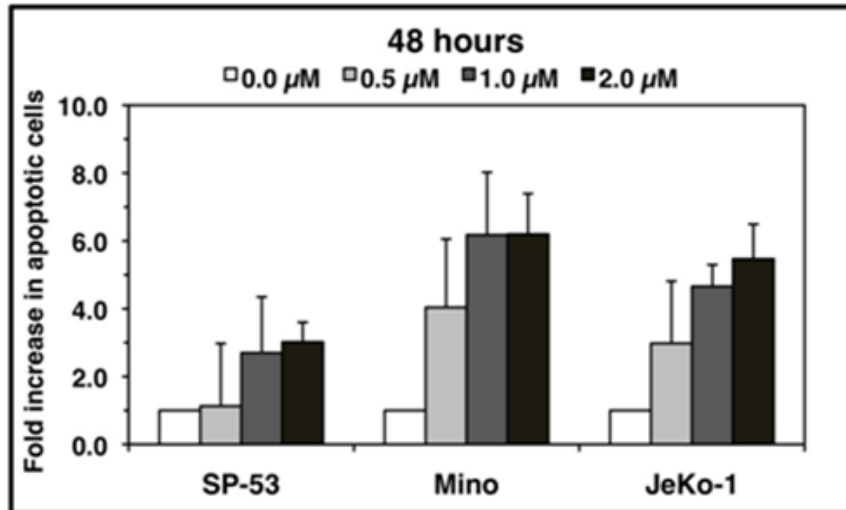
Figure 18. Induction of apoptosis in MCL by PPP: (A) MCL cells were treated with PPP using 4 different concentrations of 0, 0.5, 1.0, and 2.0 µM for 24 hours. Apoptosis was determined using Annexin-V/FITC and PI staining. Cells were considered apoptotic if they were Annexin-V+ only or Annexin-V +/PI+ and were normalized against control cells (untreated). Results show occurance of apoptosis in a concentration-dependent manner. **(B)** Apoptosis increased further after 48 hours of treatment. Results shown are means ± SD.
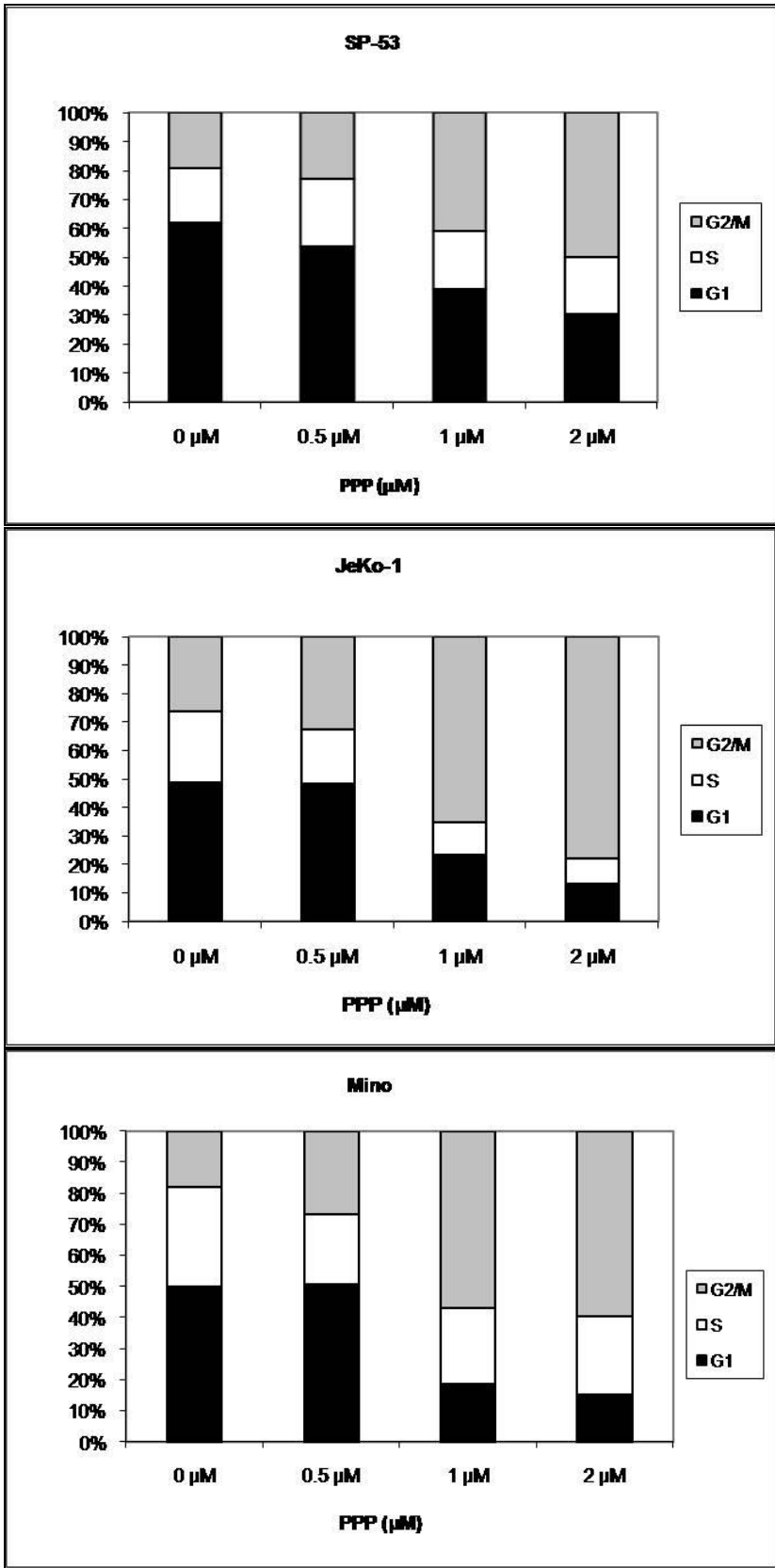
Figure 19. Analysis of cell cycle after treatment with PPP: MCL cells were treated with PPP using 4 different concentrations of 0, 0.5, 1.0, and 2.0 µM for 24 hours. Cell cycle was determined by PI staining and flow cytometry. Results show that cells undergo a G2/M-phase cell cycle arrest after treatment with PPP.
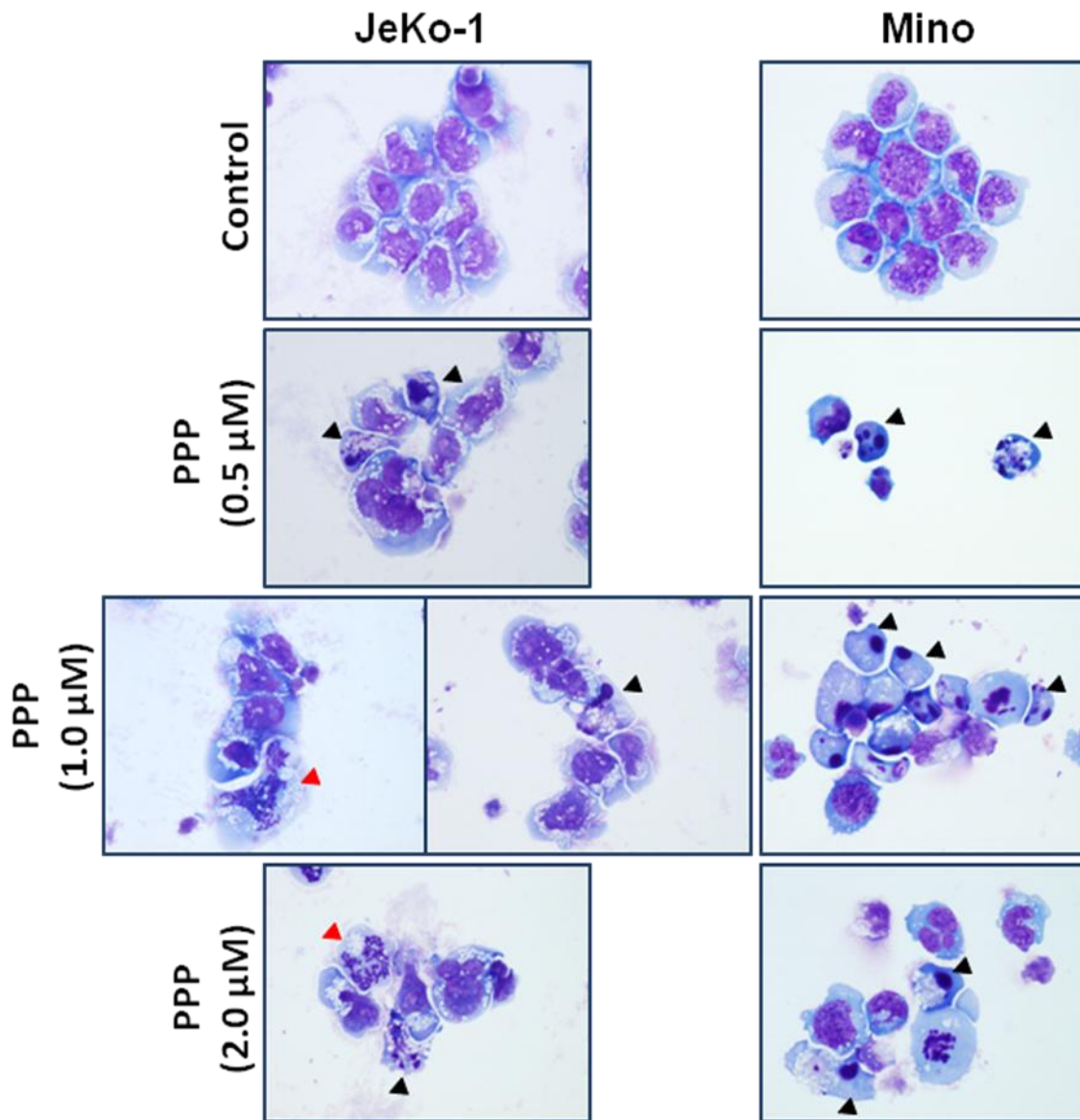
Figure 20. Morphological changes after treatment with PPP: Cytospin slides were prepared with MCL cells treated with PPP using 4 different concentrations of 0, 0.5, 1.0, and 2.0 μM for 24 hours and were stained with Geimsa. Morphological changes associated with apoptosis included nuclear fragmentation and condensation and cell shrinkage (black arrowheads) compared to control cells (untreated). Consistent with the G2/M-phase cell cycle arrest, atypical mitotic figures were seen (red arrowheads)

A.
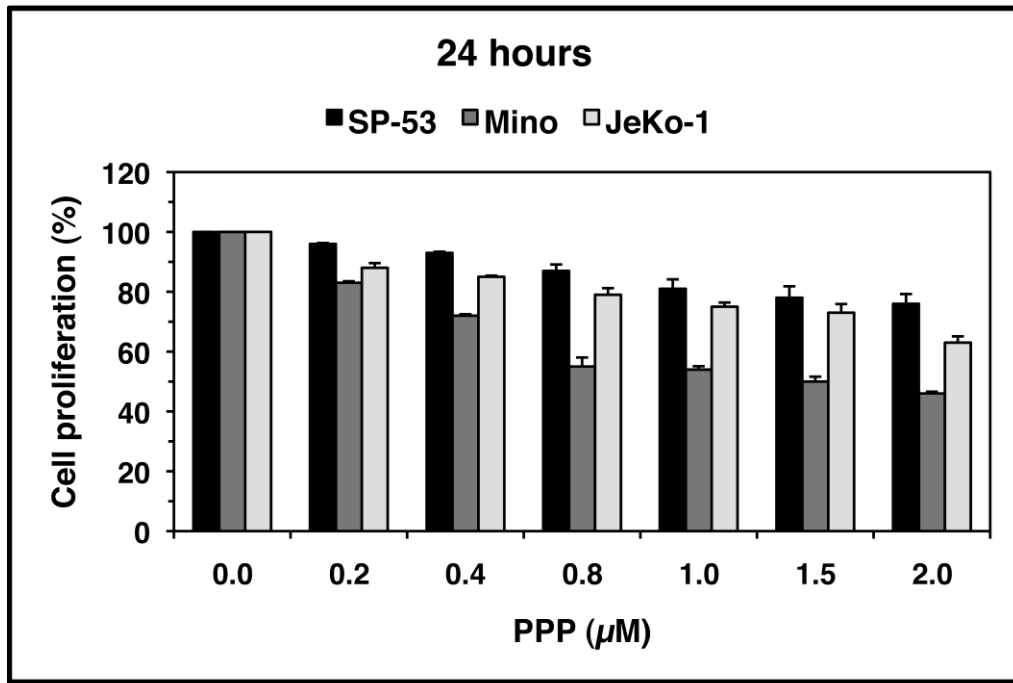
B.
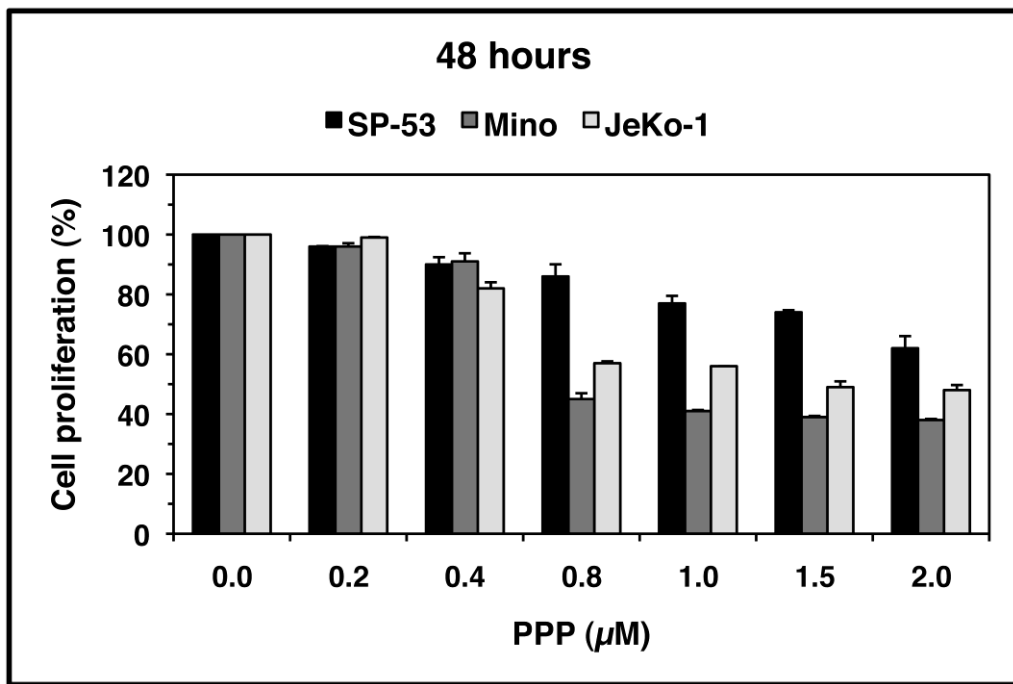
Figure 21. MTS assay after treatment with PPP: (A) MCL cells were treated with PPP for 24 hours. OD readings were taken 4 hours after MTS assay was performed. MCL cells displayed decreased cell proliferation at 24 hours which was **(B)** further enhanced at 48 hours. Results shown are means ± SD.

3.3 Biochemical effects of selective inhibition of IGF-IR by PPP

To determine the biochemical effects of inhibition of IGF-IR by PPP, we performed Western blotting analysis of downstream targets of IGF-IR using Mino cell lysates. As shown in **Figure 22**, PPP induced downregulation of phosphorylated Akt (pAkt) without significantly altering its total protein levels. In addition, PPP also induced changes in cell cycle regulatory proteins. We noticed an upregulation of cyclin B1 and downregulation of pCdc2 which are consistent with the G2/M phase cell cycle arrest. Cleavage of pro-apoptotic molecules including caspase-3 and PARP was also seen.
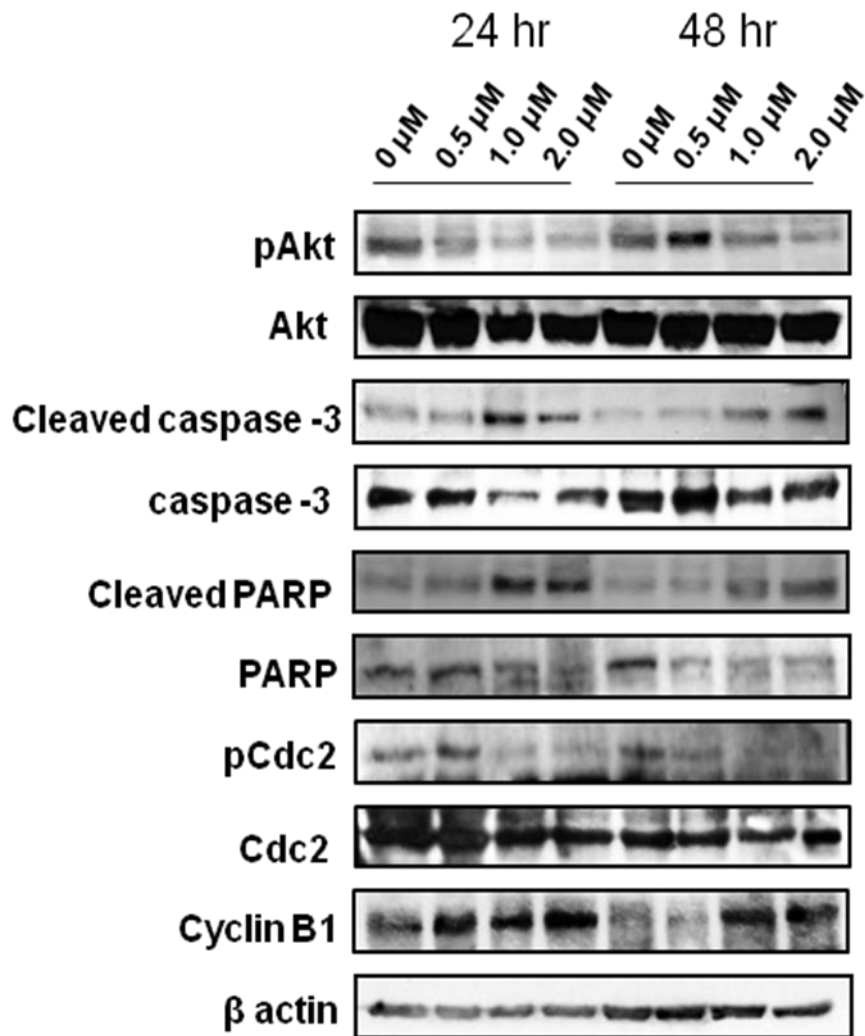
Figure 22. Downstream signaling changes associated with inhibition of IGF-IR by PPP: To assess changes in downstream signaling molecules after inhibition with PPP after 24 and 48 hours, Western blotting was utilized using Mino cell lysates. Results showed that PPP significantly downregulated phosphorylated Akt without significantly altering its total protein levels. PPP also induced changes in cell cycle regulatory proteins, including an upregulation of cyclin B1 and downregulation of pCdc2. Cleavage of pro-apoptotic molecules such as caspase-3 and PARP was also seen.

3.4 Biochemical effects of specific inhibition of IGF-IR by siRNA

Selective targeting using a small molecule inhibitor such as PPP can induce nonspecific effects, therefore, experiments based on specific approaches to further confirm the role of IGF-IR in MCL were performed using siRNA. Cells were treated with either scrambled or IGF-IR siRNA for 24 and 48 hours. At 24 hours, there was considerable knockdown of IGF-IR expression **(Figure 23A).** However, at 48 hours, there was significant knockdown of IGF-IR **(Figure 23B)**. IGF-IR siRNA significantly decreased pAkt and pJnk protein kinases. There was significant downregulation of cyclin D1. Finally, there was cleavage of pro-apoptotic molecules caspase-3 and PARP.
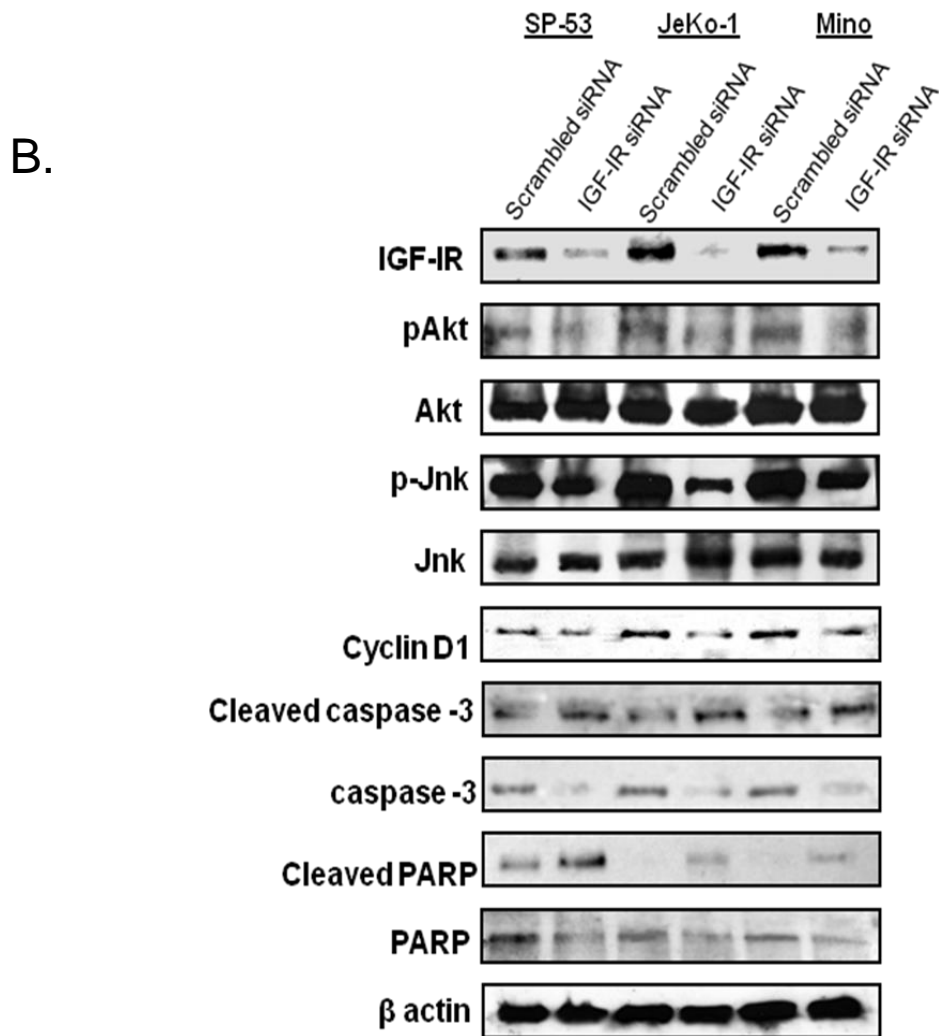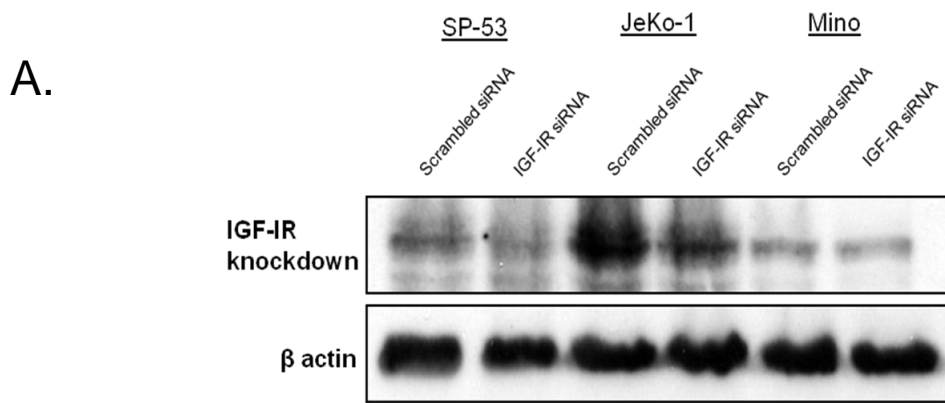
Figure 23. Downstream signaling changes associated with inhibition of IGF-IR by siRNA: **(A)** MCL cells were treated with either scrambled siRNA or IGF-IR siRNA for 24 hours. Moderate knockdown was observed in IGF-IR. **(B)** MCL cells were treated with scrambled or IGF-IR siRNA for 48 hours. Significant knockdown was observed in IGF-IR. IGF-IR siRNA significantly decreased oncogenic kinases pAkt and pJnk. There was downregulation of cyclin D1. Finally, there was cleavage of pro-apoptotic molecules such as caspase-3 and PARP.

Chapter IV: Discussion

IGF-IR and its primary ligand IGF-I have been shown to play a key role in the establishment and progression of tumors. It has been well described that overexpression of IGF-IR induces aberrant cell proliferation and malignant transformation in several cancers such as those of the prostate, breast, lung, ovaries, and soft tissue (25, 48, 49, 55, 57). Overexpressed IGF-IR can also protect cells from apoptosis in addition to promoting metastasis and upregulating proteins involved in angiogenesis, such as VEGF (60, 86, 94, 95). Investigations conducted on IGF-IR in hematological malignancies (plasma cell myeloma, leukemia, and lymphoma) are limited. To the best of our knowledge, most of the work to date has been performed on plasma cell myeloma (68, 93, 94, 96-100). As previously demonstrated in our lab, IGF-IR has shown oncogenic potential in chronic myeloid leukemia and NPM-ALK expressing T-cell lymphoma (101, 102).

In the present study, we have attempted to provide evidence that IGF-IR has an important role in maintaining the survival of mantle cell lymphoma (MCL) cells. We found that IGF-IR is overexpressed in MCL cell lines (SP-53, JeKo-1, Mino, and Granta) when compared to its expression in normal human CD19+ B-lymphocytes at both the mRNA and protein levels. All these cell lines have been previously characterized (103). SP-53 seemed to display lower levels of expression compared to JeKo-1 and Mino. In these experiments, the mouse fibroblast cell lines P6 and R- were used as positive and negative controls, respectively. The P6 cell line is derived from BALB/c3T3 cells expressing a human IGF-IR sequence (Cvn-IGF-IR) under the control of the simian virus 40 (SV40) large T antigen promoter and therefore, is induced to overexpress IGF-IR (104, 105). R- is another cell line derived from BALB/c3T3 cells that were originally developed in mice after targeted ablation of IGF-IR (104, 105). R- was first discovered to be incapable of being transformed by the SV40 large T antigen virus (105). While the R- cell line displayed no IGF-IRα mRNA, it displayed very low expression of the IGF-IRβ subunit. Previous studies conducted in our lab, as well as in others (59, 101, 102), have shown that some R-

57

subclones exhibit low levels of IGF-IRβ subunit; however, since it lacks the IGF-IRα subunit, this low level of IGF-IRβ expression most likely has no functional implication. Moreover, R- did not display any IGF-IR protein expression. Immunohistochemistry and immunofluorescence revealed IGF-IR to be mostly localized in the cell membrane, with some cytoplasmic staining in all 3 cell lines.

Although a mechanism of overexpression of IGF-IR in tumor cells has yet to be elucidated, it has been previously shown that the number of IGF-IR molecules per cell plays a key role in the transforming properties of IGF-IR. In fibroblasts, an IGF-IR number greater than 20,000 per cell is needed to induce mitosis after stimulation with IGF-I (59). Similarly, in MCF-7, the breast carcinoma cell line, IGF-I acquires mitogenic properties after the number of IGF-IR has been increased by treatment with estrogen (106). It has also been reported that in a pancreatic cell line model, an increase in receptor number from 40,000 receptors/cell to 100,000 receptors/cell is in the range required to enable IGF-I dependent mitogenisis and therefore may be of central importance for pancreatic tumor growth control (61). Based on these findings, it is concluded that only a small increment in the number of IGF-IR molecules per cell can induce transformation of different types of tumor cells. In this study, we analyzed relative antigen density of IGF-IR receptors per cell in MCL cell lines without any exogenous stimulation by IGF-I (except IGF-I present in FBS). All 3 cell lines displayed up to 400-fold higher number of IGF-IR molecules/cell relative to normal human B-lymphoctyes. Consistent with our results showing mRNA and protein expression, SP-53 showed a lower number of receptors/cell compared to JeKo-1 and Mino.

Although overexpression of IGF-IR is an important feature for the transformation of cells, it is not necessarily the sole contributor. Another important aspect is the status of phosphorylation/activation in the receptors. Because we found overexpression of IGF-IR in SP-53, JeKo-1, and Mino, we explored whether the receptor was phosphorylated/activated in these cells. Immunoprecipitation revealed all 3 cell lines being phosphorylated; SP-53

having lower levels of phosphorylation relative to JeKo-1 and Mino. Since both

phosphorylation status and number of receptors/cell play important roles in maintaining the

transforming properties of IGF-IR, the interesting observation of SP-53 having lower

number of receptors/cell as well as lower phosphorylation status could possibly suggest

that the IGF-I-axis is not as functional as it may be in the other two MCL cell lines, JeKo-1

and Mino.

IGF-I is the primary ligand to IGF-IR. Previous studies have proposed both IGF-I-

dependent mechanisms through ligand-receptor interaction as well as IGF-I-independent

mechanisms through a constitutively active receptor (58, 107). In the IGF-I-dependent

mechanism, ligand binding results in the autophosphorylation of tyrosine residues in the β

subunit and activation of the kinase domain of IGF-IR, allowing for its substrates IRS-I or

Shc protein (among others) to bind. Binding of its substrates induces downstream signaling

cascades via PI3K/Akt and MAPK pathways (36). Therefore, we wanted to determine

whether the activation of IGF-IR in MCL cells was at least partially due to the release of

IGF-I. We tested the expression of IGF-I mRNA using RT-PCR and quantitative real time

PCR and found no apparent expression by either method. Therefore, paracrine stimulation,

for example through release of IGF-I from stromal cells, likely accounts for stimulation of

IGF-IR in MCL cells (107). Similarly, a high concentration of circulating IGF-I may facilitate

growth of MCL cells via IGF-IR as it has been previously documented in other types of

cancer (107). At this point, the status of circulating IGF-I levels in MCL patients is not

known.

Although MCL cells seem to lack autocrine release of IGF-I, we wanted to next

determine whether the cells would respond to exogenous addition of IGF-I and determine if

the IGF-IR signaling axis is indeed functional. When serum starved MCL cells were treated

with increasing concentrations of exogenous IGF-I, apoptosis decreased in comparison to

untreated starved and unstarved cells perhaps by IGF-I rescuing the MCL cells. This

suggests that IGF-IR can respond to IGF-I and that IGF-IR signaling axis is functional in MCL. Importantly, the effects exerted by IGF-I were diminished upon addition of an IGF-IR blocking antibody. This is especially important in ruling out the effects seen upon treatment with IGF-I are being induced through the insulin receptor (IR). We also observed that cells treated with IGF-I and anti-IGF-IR blocking antibody together exhibited more apoptosis than that of the starved cells control. This may imply that the IGF-IR blocking antibody induces some cytotoxic effects; however, these effects were less than 5% and therefore can be considered negligible.

The significance of whether the functionality of IGF-IR is important for the survival of MCL was demonstrated through experiments showing selective inhibition of the receptor using the cyclolignan picropodophyllin, PPP. PPP has been shown to be an activation-loop small molecule inhibitor of IGF-IR. In a very recent study, PPP was also found to be the most efficient in killing uveal melanoma cells after oral administration in a SCID mouse model (91). PPP was well tolerated by the animals and also decreased VEGF expression in the tumors. It was demonstrated previously that PPP is an inhibitor of the IGF-IR tyrosine phosphorylation and importantly it did not interfere with the highly homologous IR (84, 90). It was shown that PPP did not selectively inhibit the IGF-IR tyrosine kinase at the level of ATP binding. This suggests that it acted through suppression of other components, such as at the level of receptor substrate. Although the effects of PPP on other kinases are not completely known, our lab recently demonstrated that PPP does not affect BCR-ABL phosphorylation level or tyrosine kinase activity (101) .

After treatment of MCL cells using an increasing concentration range of PPP, we found reduced phosphorylated levels of IGF-IR in a concentration-dependent manner. Furthermore, IGF-IR tyrosine kinase activity also decreased in a similar fashion. As mentioned earlier, PPP has been shown to be an activation-loop small molecule inhibitor of IGF-IR. IGF-IR, in its inactive state, contains the activation loop which houses the critical

tyrosine residues 1131, 1135, and 1136. Y1135 (being the first tyrosine to be

phosphorylated) in the activation loop is bound in a *cis* position and therefore prevents any

access by the substrates or ATP. After ligand binding, the three tyrosines of the activation

loop are phosphorylated to a *trans* position in the β subunit. Phosphorylation of Y1135 and

Y1131 destabilizes the autoinhibitory conformation of the activation loop, while

phosphorylation of Y1136 residue stabilizes the active conformation of IGF-IR (92). These

changes in the activation loop conformation allow for substrate and ATP binding and

subsequent activation of downstream signaling of IGF-IR. PPP is said to selectively inhibit

phosphorylation of Y1136 of the activation loop while refraining from Y1131 and Y1135.

Although there is a possibility that inhibition of Y1136 phosphorylation is insufficient to

completely eliminate total tyrosine activity of IGF-IR, the important feature to note is that the

lack of Y1136 itself may decrease the overall kinase activity of IGF-IR since Y1136

stabilizes IGF-IR and is therefore a necessity in obtaining full kinase activity (92).

When we sought to determine the effects of downregulation of IGF-IR signaling by

PPP, we found a decrease in cell viability, a decrease cell proliferation, induction of

apoptosis, and G2/M-phase cell cycle arrest in a concentration- dependent manner.

Additionally, we observed changes in downstream signaling proteins after PPP treatment.

To rule out the possibly of nonspecific effects of PPP, we also explored specific targeting of

IGF-IR using siRNA. Knockdown with IGF-IR siRNA confirmed the results obtained by PPP

inhibition regarding the changes to several key downstream signaling proteins that are

essential for MCL pathogenesis. In our study, MCL cells revealed downregulation of pAkt

after targeting IGF-IR, without significantly altering baseline expression or total protein.

Previous studies have shown that a single mutation in Y1136 of IGF-IR (Y1136F) almost

completely terminated the Akt phosphorylation and that Y1136F also reduced

phosphorylation of IRS-1, the IGF-IR substrate that induces the PI3K/Akt pathway. This

suggests that this residue is especially important for the PI3K/Akt pathway and that another

mode of downregulation of IGF-IR is through downregulation of pIRS-I after blockade of Y1136 (87). Since IGF-IR also induces its effects through the MAPK pathway, we studied proteins involved in this pathway. We observed decrease in pJnk, a member of the MAPK group that is activated by phosphorylation on both threonine and tyrosine residues. Jnk signaling pathway is said to be structurally similar to the Erk pathway and is activated by the GTP binding protein Ras via Raf and MEK1 protein kinase cascade (108, 109).

Along with downregulation of activated forms of oncogenic kinases, there were changes in apoptotic molecules as well. IGF-IR has previously been shown to inhibit apoptosis by inhibiting release of cytochrome C through the activation of the PI3K/Akt pathway (74, 75). Activated Akt can phosphorylate the pro-apoptotic protein Bad (74). Upon phosphorylation, Bad is dissociated from anti-apoptotic Bcl-2, and becomes temporarily controlled by the adaptor protein 14-3-3. If Bad is not phosphorylated, other pro-apoptotic proteins, such as Bak and Bax, become activated and cause cytochrome C release from mitochondria. In turn, caspase-9 and then caspase-3 become activated (75). Activated caspase-3 can cleave and inactivate, for example, the poly(ADP-ribose) polymerase (PARP), which normally functions in DNA repair and programmed cell death (75) and this results in extensive degradation of DNA at the final steps in the apoptotic process. Although we saw a downregulation of pAkt, we did not see any changes in anti-apoptotic molecules Bcl-2 and Bcl-xL (data not shown). However, we did see cleavage of caspase-3 and PARP. In addition, siRNA confirmed the activation of the pro-apoptotic molecules that was observed with PPP treatment.

Finally, we detected changes in cell cycle regulatory molecules, including those involved in the G2/M-phase cell cycle arrest. It has previously been shown that PPP exerts cell cycle arrest at this stage (93, 101, 102). IGF-IR can regulate cell cycle progression at several phases, but its major direct role is seen at the earlier stages of the cell cycle. It can exert its effects at the G_0/G1 phase through the activation of p70 S6K, a protein Ser-Thr

kinase that phosphorylates the S6 ribosomal subunit necessary for entry into the next phase of the cell cycle (69). In the G1/S phase, IGF-IR can increase cyclin D1 and CDK4 gene expression primarily through the PI3K/Akt and/or ERK pathways, leading to inactivation of Rb1 protein, allowing E2F transcription factors to be released (69). Finally at the G2/M-phase, it has been shown that IGF-IR can regulate cyclins A and B as well as promote synthesis of Cdc2 (69). In our study, we found downregulation of pCdc2 and a simultaneous upregulation of cyclin B1. In a normal cell, cyclin B1 is a regulatory protein having roles in mitosis. It complexes with p34(cdc2) to form the maturation-promoting factor (MPF) that induces entry into the G2/M phase of the cell cycle. Throughout the cell cycle, cyclin B1 accumulates but is only activated after dephosphorylation by the phosphotase Cdc25. It is degraded at the end of mitosis and accumulates again during the next cell cycle (110). The changes in these proteins we observed in our study might imply an interference between cyclin B1 and pCdc2. Effects of inhibition of IGF-IR by PPP probably induces dephosphorylation of Cdc2 and in turn prevents cyclin B1 from forming the MPF complex, causing it to accumulate and render G2/M phase cell cycle arrest.

A recent study showed the differential effects of A12, an anti-IGF-IR antibody, on cell cycle in androgen-dependent (AD) and androgen-independent (AI) prostate cancer (111). It was demonstrated that A12 induced a G1-phase cell cycle arrest in AD tumors and a G2/M-phase cell cycle arrest in AI prostate tumors, testifying to the fact that IGF-IR inhibition can result in cell cycle arrest at any phase of the cell cycle. Previously in our lab, we also demonstrated decrease in cyclin E, another G1/S-phase regulator, after treating chronic myeloid leukemia cell lines with PPP (101). In spite of evidence to support regulation of the early stages of the cell cycle by IGF-IR, it was interesting to find only a G2/M-phase cell cycle arrest after inhibition with PPP in our study. One explanation might be the possibility of PPP inducing a G2/M-phase cell cycle arrest independent of IGF-IR through mechanisms that are still not fully understood. Another explanation may be that proteins

63

involved in regulating the early and later stages of the cell cycle maintain a specific balance in activity that is required for proper cell cycle progression. In our study, after inhibiting IGF-IR we saw downregulation of cyclin D1, the key cell cycle regulatory molecule that is upregulated in MCL due to the t(11;14)(q13;q32) translocation. This data might suggest that a decrease in expression of proteins involved in earlier phases of the cell cycle might disrupt the normal balance, resulting in the accumulation of G2/M-phase regulatory proteins. In addition, the loss in interaction between G2/M-phase regulatory proteins, such as cyclin B1 and Cdc2, may also contribute to the final arrest at the later phase of the cell cycle. As previously mentioned, IGF-IR regulates the G2/M-phase by promoting synthesis of Cdc2. The effects of apoptosis and cell cycle arrest were consistent with the morphological changes observed by Geimsa staining of MCL cells after treatment with PPP, showing nuclear fragmentation, cell shrinkage, and increase in abnormal mitotic figures.

In conclusion, we provide evidence to show that IGF-IR plays an important role in maintaining the survival of MCL. Interestingly, the experiments showed SP-53 to be generally the more resistant cell line and JeKo-1 and Mino to be the more sensitive cell lines to the inhibition of IGF-IR. This could perhaps be linked to the lower expression and phosphorylation of IGF-IR in SP-53. The lower expression levels may not be sufficient to fully utilize the IGF-IR axis and therefore, SP-53 cells do not respond as prominently as the other two cell lines, JeKo-1 and Mino to inhibition of IGF-IR. We found that inhibition of IGF-IR induces cell death in MCL cell lines possibly through downregulation of phosphorylation of Akt, Jnk, and cyclin D1 and disrupting the interactions between cell cycle regulating complex cyclin B1/Cdc2 to result in a G2/M-phase cell cycle arrest. In addition, inhibition of IGF-IR facilitates the cleavage, and thus the activation of pro-apoptotic molecules such as caspase -3 and PARP. Taken together, our studies suggest that IGF-IR

plays a role in the pathogenesis of MCL and therefore, it might represent a potential

therapeutic target that could be utilized in treating MCL in the future.

Chapter V: Methods and Materials

Cell lines:

Four characterized MCL cell lines were used in this study including SP-53, Mino, JeKo-1, and Granta 519 (103). The P6 (mouse BALB/c3T3 fibroblasts overexpressing human IGF-IR) and R- (mouse 3T3-like fibroblasts with targeted ablation of _Igf1r_) cell lines were a generous gift from Dr. R. Baserga (Thomas Jefferson University, Philadelphia, PA) and were used as positive and negative controls for experiments showing expression of IGF-IR, respectively (101, 102, 104, 105). In some experiments, the ALK+ ALCL cell line Karpas 299 was used additionally as a positive control for the expression of IGF-IR (102). The normal human skin fibroblast cell line AG01523 (Coriell Institute for Medical Research, Camden, NJ) was used as a negative control for PPP treatment experiments (93). MCL cell lines were maintained in Roswell Park Memorial Institute 1640 (RPMI 1640) medium (HyClone, South Logan, Utah) supplemented with 15% fetal bovine serum (FBS; Sigma, St. Louis, MO), glutamine (2 mM), penicillin (100 U/ml), and streptomycin (100 µg/ml) at 37°C in a humidified 5% CO_2 in air chamber. Dulbecco's Modified Eagle Medium (DMEM) (P6 and R-), RPMI (Karpas 299), or Minimum Essential Medium (Eagle) in Earle BSS (EEMEM) (AG01523) supplemented with 10% FBS were used to culture the cells under the same above conditions.

Antibodies:

Antibodies used from Santa Cruz Biotechnology (Santa Cruz, CA) included cyclin B1 (sc-7393), Cdc2 (sc-52316), pCdc2 (Thr14/Tyr15;sc-12340-R), and p-Tyr (PY99; sc-7020); from Cell Signaling Technology (Danvers, MA) were Akt (9272), and pAkt (Ser473; 9271S), caspase-3 (total) (9668), caspase-3 (cleaved) (9661), pJnk (9255), and Jnk (9252); from Zymed Laboratories (South San Francisco, CA) was IGF-IRβ (39-6700); from Sigma (St. Louis, MO) was β-actin (A-2228); from BD Biosciences (San Jose, California) were PARP (total) (556362), PARP (cleaved) (552596).

The cyclolignan picropodophyllin (PPP) was purchased from Calbiochem (Gibbstown, NJ, catalog # 407247). PPP was prepared and dissolved in ethanol to a final concentration of 0.5 mM (amount of ethanol was less than 0.4% by volume and therefore had no affect on treated cells).

For treatment of MCL cell lines with PPP, cells were incubated at 37°C in 5% CO_2 in humidified air. Cells were collected, centrifuged at 300x *g*, washed twice in sterile 1x PBS, and seeded at concentrations appropriate for experiment. PPP was added at concentrations ranging from 0.2-2 µM for 24 hours or 48 hours. As a negative control, untreated cells were seeded for each concentration simultaneously.

For IGF-IR knockdown experiments with siRNA, specific targeting of IGF-IR was achieved by transient transfection with SMARTpool designed siRNA (mixture of 4 different constructs) (Dharmacon, Lafayette, CO, M-003012-04). The siCONTROL Non-Targeting siRNA was used as a negative control (Dharmacon, Lafayette, CO, D-001206-13-20). Transfection of the cells by siRNA was performed using the Nucleofector "R" solution for JeKo-1 or "T" solution for Mino and SP-53 as recommended by the manufacturer (Amaxa Biosystems; A-023 program for JeKo-1, T-001 for Mino, and O-017 for SP-53). Briefly, 2 x 10^6 cells per nucleofection sample was resuspended in appropriate nucleofector solution at a final concentration of 2 x 10^6 cells/100 µl. 20 µM IGF-IR siRNA or 20 µM scramble siRNA were added to the mixture. The mixture was placed in a cuvette and electroporation was performed using an Amaxa electroporation system (Basel, Switzerland, catalog #AAD-1001). Once electroporation was complete, the mixture was transferred into a 6-well plate containing 500 µl of pre-warmed RPMI 1640 supplemented with 15% FBS. Cells were

incubated for 24 hours or 48 hours after transfection at 37°C in a humidified 5% CO_2 in air chamber.

The response of MCL cells to IGF-I was detected by cell viability. Because IGF-I is present in FBS, 4.0×10^5 cells/mL were collected by centrifugation, washed once with 1x sterile PBS, and maintained in serum-free medium. Simultaneously, cells were treated with 500 ng/mL of IGF-I (291-G1-050; R&D systems) with or without an anti-IGF-IR blocking antibody at a concentration of 5 µg/mLfor 24 hours. Immediately thereafter, cell viability was analyzed using exclusion of staining by trypan blue dye.

Exclusion of staining by trypan blue dye assay:
Cell viability was measured using exclusion of staining by trypan blue dye. Approximately, 100 µl of cells were mixed with equal volume trypan blue and resuspended. 10 µl of resuspended cells were analyzed using a hemocytometer.

Reverse transcriptase polymerase chain reaction (RT-PCR):
RT-PCR was used to determine the expression of IGF-IR mRNA. Total RNA was isolated and purified using RNAeasy Mini Kit (Qiagen, Valencia, CA). Briefly, 1×10^6 cells were collected by centrifugation at 300x *g* for 5 minutes, washed twice in sterile 1x PBS, and subjected to lysis and homogenization by RLT buffer (RNA Lysis Buffer). Homogenized cells were passed through provided spin columns and washed once with 70% ethanol. Two additional washing steps were performed with appropriate buffers. Total RNA was collected upon elution with RNAse-free water. Optical density readings were read using DNA/Protein Analyzer (Beckman Coulter, Fullerton, CA)

Reverse transcription was performed through a two-step procedure using ThermoScript RT protocol (Invitrogen, Carlsbad, CA). Approximately 0.3 μg total RNA was used for reverse transcription. First, total RNA, oligo (dT), and dNTP mix were added to a mixture that was adjusted to a final volume of 12 μl with DEPC-treated water. RNA mixture and primer was denatured by incubating at 65°C for 5 min and then placed on ice.   Second, a master reaction mix consisting of 5x cDNA synthesis buffer, 0.1 DTT, RNaseOUT, Thermoscript RT, and DEPC-treated water was prepared on ice and vortexed gently. Approximately 8 μl of reaction mix was pipeted into each reaction tube on ice bringing final volume to 20 μl. The samples were then transferred to a thermal cycler preheated to the appropriate cDNA synthesis temperature and incubated for 60 minutes at 50°C, then terminated at 85°C for 5 minutes. 1 μl of RNase H was added and incubated at 37°C for 20 min. 20 μl PCR reactions were performed using HotStar Master Mix kit (Qiagen).

The primers used for RT-PCR are summarized in the following table:

Primers and Conditions	
IGF-IRα (product size 307bp)	
Forward	5'-GTAGCTTGCCGCCACTACTACT-3'
Reverse	5'-GGAGCATCTGAGCAGAAGTAACAGA-3'
Amplification (35 cycles)	94°C (30 seconds), 58°C (30 seconds), 72°C (30 seconds)
Final elongation	72°C (10 minutes)
IGF-IRβ (product size 450 bp)	
Forward	5'-TGGGGAAGGAGTGCTGTAT-3'
Reverse	5'-CGGCCATCTCTGAATCATCTTG-3'
Amplification (35 cycles)	94°C (60 seconds), 56°C (60 seconds), 72°C (60 seconds)
Final elongation	72°C (10 minutes)
IGF-I (product size 413 bp)	
Forward	5'-TCCTCGCATCTCTTCTACC-3'
Reverse	5'-TGGCATGTCACTCTTCACT-3'
Amplification (35 cycles)	94°C (60 seconds), 58°C (60 seconds), 72°C (60 seconds)
Final Elongation	72°C (10 minutes)
IGF-I (product size 299 bp)	
Forward	5'-GAAGGTGAAGATGCACACCA-3'
Reverse	5'-AGCGAGCTGACTTGGCAGGCTTGA-3'
Amplification (35 cycles)	94°C (60 seconds), 63°C (40 seconds), 72°C (60 seconds)
Final Elongation	72°C (10 minutes)

β-actin (RDP-38, R&D Systems) was used as an internal control (primer sequence not provided by the manufacturer).

The PCR products were detected by ethidium bromide staining on a 1.5% agarose gel and visualized by FluorChem 8800 imaging system (Alpha Innotech).

Quantitative real time polymerase chain reaction:

Quantitative real-time PCR was used to examine levels of IGF-I mRNA in MCL cell lines. The primer/probe sets used were obtained from Applied Biosystems (sequences not provided):

Primer/Probe Set	Catalog Number
18S	4319413E-0402011
IGF-IR	Hs00181385_m1; Lot#: 489925
IGF-I	Hs01547657_m1; Lot#: 654623

Western blotting and immunoprecipitation:

Western blotting was used to analyze the expression of proteins and other signaling molecules directly downstream of IGF-IR. Cells were collected and lysed using lysis buffer containing 25 mM HEPES (pH 7.7), 400 mM NaCl, 1.5 mM $MgCl_2$, 2 mM EDTA, 0.5% Triton X-100, 0.1 mM PMSF, 2 mM DTT, phosphatase inhibitor (20 mM B-GP, 1 mM Na3VO4, Roche), and protease inhibitor cocktails (10 µg/ml leupeptine, 2 µg/ml pepstatin, 50 µg/ml antipain, 1x benzamidine, 2 µg/ml chymostatin; Roche). Concentrations were measured using Bio-Rad protein assay and OD values were obtained using an ELISA plate reader (Bio-Tek Instruments, Winooski, VT). Proteins (50µg) were electrophoresed on 8% SDS-PAGE. The proteins were transferred to nitrocellulose membranes and probed with specific primary antibodies and then with appropriate horseradish peroxidase-conjugated secondary antibodies (Santa Cruz; and GE Healthcare,Cardiff, UK). Proteins were detected using chemiluminescence-based kit (Amersham Life Sciences, Arlington Heights, IL).

Immunoprecipitation was performed by adding total protein extracts (800 µg) to agarose beads conjugated with A/G and pre-cleared to remove non-specific binding proteins to these agaroses by shaking gently at 4°C for 20 minutes. The lysates were spun at 4°C for 10 min at 10,000x *g*, and supernatant was collected. IGF-IRβ antibody (2.5 – 5 µg) was

added to supernatant and incubated overnight at 4°C. Agarose beads conjugated with A/G

were then added to the supernatant and incubated additionally for 4 hours at 4°C. The

lysates were spun at 4°C for 1 minute at 10,000x g and supernatant was removed. The

beads were washed 3 times with cold 1x PBS and once with lysis buffer, and then

subjected to SDS-PAGE. The membrane was subsequently stained with anti-p-Tyr

antibody or IGF-IR antibody.

Flow Cytometry:

Quantitative analysis of IGF-IR expression by assessing relative antigen density of IGF-IR

(FACscan, BD Pharmingen, San Jose, CA) was performed using flow cytometry and the

QuantiBrite PE kit (BD Biosciences, Franklin Lakes, NJ). Briefly, $1x10^6$ cells were

collected, washed once 1x PBS, and incubated for 30 minutes at room temperature in the

dark with either PE-labeled anti-human IGF-IR antibody (555999; BD Biosciences, San

Jose, CA) or PE-labeled anti-mouse IgG1 isotype control (555749; BD Biosciences). Cells

were then washed twice with ice cold 1x PBS and subjected to immediate analysis by

CELLQuest™ software (BD Immunocytometry Systems, Oakville, Ontario, Canada).

Calibration beads were first reconstituted using 0.5 mL PBS with 0.5% BSA and vortexed.

Calibration and regression analysis were performed using the QuantiBrite beads and the

parameters were adjusted appropriately for cellular assay. Data acquisition was performed

using these same settings. PE-conjugated IGF-IR molecules per cell were manually

calculated considering that the PE: mAb ratio was 1:1 using Excel according to the

manufacturer's instructions.

Apoptosis was determined using flow cytometry analysis (FACscan, BD Pharmingen, San

Jose, CA) after staining the cells with annexin V-FITC and propidium iodide (PI) (BD

Pharmingen) and cell cycle analysis was examined using CycleTEST PLUS DNA reagent kit (BD, Pharmingen).

Immunohistochemistry:

Immunohistochemical techniques using DakoCytomation kit (DakoCytomation, Carpinteria, CA) were performed on formalin-fixed paraffin embedded sections obtained from cell blocks of cell lines. Briefly, sections were deparaffinized by incubating the slides in:

1. Xylene (2 x 5 min)
2. 100% Ethanol (3 x 5 min)
3. 95% Ethanol (3 x 5 min)
4. 80% Ethanol (3 x 5 min)

After washing in 1x PBS twice, slides were placed in pre-warmed retrieval solution (provided in kit) in a steamer for 45 minutes. Tissue was incubated with hydrogen peroxide for 15 minutes at room temperature, and then subjected to washing three times with PBS for 5 minutes each. Slides were then blocked with blocking buffer for 30 minutes and incubated overnight at 4°C with IGF-IRβ antibody at a dilution of 1:30 diluted in same blocking buffer. Sequentially, slides were washed 3 times for 10 minutes and incubated with secondary antibody LINK and then with secondary antibody Streptavidin each for 30 minutes. Slides were then developed with 3,3´-diaminodbenzidine tetrahydrochloride substrate kit (DAB) that includes horseradish peroxidase enzyme (HRP) for 4 minutes and hematoxylin was used for counter staining. Photomicrographs were obtained using a Nikon Microphot FXA microscope (Nikon Instruments, Melville, NY) and an Olympus DP70 camera (Olympus America, Melville, NY).

Cytospins for morphological studies were prepared using approximately 100,000 cells loaded into cytospin machine (Shannon Cytospin, Medway, MA). Slides were further stained with Giemsa and examined by light microscopy (Olympus, Center Valley, PA) to confirm morphological changes correlating with apoptosis and cell cycle arrest.

For confocal laser-scanning electron microscopy, cytospin slides (MCL cells, R- and Karpas 299) were washed once with PBS and subjected to a fixation-permeabilization step in 4% paraformaldehyde for 20 minutes, followed by 20 minutes in 0.1% Triton X-100 at room temperature. After blocking with 10% FBS in PBS for 45 minutes, cells were incubated with a rabbit anti–IGF-IRβ antibody (1:100) overnight at 4°C and stained for 90 min with secondary Cy3-conjμgated anti-rabbit IgG (1:800) (Jackson ImmunoResearch Laboratories, West Grove, PA). Images were visualized by confocal laser-scanning microscopy (LSM 510; Carl Zeiss MicroImaging, Thornwood, NY).

Tyrosine Kinase Activity:

Tyrosine kinase activity was measured using Universal Tyrosine Kinase Assay Kit (Takara Bio Inc, Pittsburg, PA). First, samples were prepared by collecting approximately 3×10^6 cells by centrifugation, washing once with PBS for 5 minutes at 300x *g* to recover as a pellet. 1 ml of extraction buffer (provided in the kit) was used to resuspend the pellet. The mixture was spun for 10 minutes at 4°C at 10,000x *g*, and the recovered supernatant was used as the sample. Using prepared cell lysates, the specific antibody for IGF-IRβ was used for the following immunoprecipitation steps. Agarose beads conjugated with protein A/G were added and immunoprecipitated. 150 µl of Kinase reaction solution including 2-mercaptoethanol was added and resuspended. This suspension was used as the samples for the measurement of PTK activity at 50 µl/ well. In order to start the phosphorylation process of tyrosine, approximately 10 µl of 40 mM ATP-2Na solution was added to 40 µl of

sample in a 96 well plate and incubated for 30 minutes at 37°C. The wells were washed 4 times with washing buffer provided in kit. Sequentially, the samples were blocked with blocking buffer for 30 minutes at 37°C. Immediately following, the anti-p-Tyr (PY20)-HRP antibody (provided with the kit) was added to the well and incubated at 37°C for 30 minutes. Upon washing the wells 4 times with wash buffer, 100µl of HRP substrate solution Tetramethylbenzidine (TMBZ) was added for 15 minutes at 37°C. The reaction was then stopped with stop solution (1N H_2SO_4) and OD readings were measured at 450 nm wavelength using an ELISA plate reader.

MTS assay:

Cell proliferation was evaluated by CellTiter 96[®] AQ_{ueous} One Solution Cell Proliferation Assay (MTS) kit (Promega). MCL cells were seeded in 96 well plates at a concentration of 10,000 cells/well in 100 µl of RPMI supplemented with 20% FBS. 20 µl of MTS reagent was added and then incubated at 37°C in a humidified 5% CO_2 in-air chamber for approximately 4 hours. OD measurements were obtained using an ELISA plate reader.

Chapter VI: References

1. Fernandez, V., E. Hartmann, G. Ott, E. Campo, and A. Rosenwald. 2005. Pathogenesis of mantle-cell lymphoma: all oncogenic roads lead to dysregulation of cell cycle and DNA damage response pathways. J Clin Oncol 23:6364-6369.

2. Johnson, K., K. L. Reddy, and H. Singh. 2009. Molecular pathways and mechanisms regulating the recombination of immunoglobulin genes during B-lymphocyte development. Adv Exp Med Biol 650:133-147.

3. Jares, P., D. Colomer, and E. Campo. 2007. Genetic and molecular pathogenesis of mantle cell lymphoma: perspectives for new targeted therapeutics. Nat Rev Cancer 7:750-762.

4. Zvara, A., L. Hackler, Jr., Z. B. Nagy, T. Micsik, and L. G. Puskas. 2002. New molecular methods for classification, diagnosis and therapy prediction of hematological malignancies. Pathol Oncol Res 8:231-240.

5. Simpson, J. F., D. E. Quan, F. O'Malley, T. Odom-Maryon, and P. E. Clarke. 1997. Amplification of CCND1 and expression of its protein product, cyclin D1, in ductal carcinoma in situ of the breast. Am J Pathol 151:161-168.

6. Betticher, D. C., J. Heighway, P. S. Hasleton, H. J. Altermatt, W. D. Ryder, T. Cerny, and N. Thatcher. 1996. Prognostic significance of CCND1 (cyclin D1) overexpression in primary resected non-small-cell lung cancer. Br J Cancer 73:294-300.

7. Sukov, W. R., R. P. Ketterling, D. J. Lager, A. W. Carlson, J. P. Sinnwell, G. K. Chow, R. B. Jenkins, and J. C. Cheville. 2009. CCND1 rearrangements and cyclin D1 overexpression in renal oncocytomas: frequency, clinicopathologic features, and utility in differentiation from chromophobe renal cell carcinoma. Hum Pathol 40:1296-1303.

8.   Kim, S. H., J. J. Lewis, M. F. Brennan, J. M. Woodruff, M. Dudas, and C. Cordon-Cardo. 1998. Overexpression of cyclin D1 is associated with poor prognosis in extremity soft-tissue sarcomas. Clin Cancer Res 4:2377-2382.

9.   Garner, E., and V. Costanzo. 2009. Studying the DNA damage response using in vitro model systems. DNA Repair (Amst) 8:1025-1037.

10.   Rudelius, M., S. Pittaluga, S. Nishizuka, T. H. Pham, F. Fend, E. S. Jaffe, L. Quintanilla-Martinez, and M. Raffeld. 2006. Constitutive activation of Akt contributes to the pathogenesis and survival of mantle cell lymphoma. Blood 108:1668-1676.

11.   Martin, P., and J. P. Leonard. 2007. Novel therapeutic targets in mantle cell lymphoma. Expert Opin Ther Targets 11:929-940.

12.   Witzig, T. E. 2005. Current treatment approaches for mantle-cell lymphoma. J Clin Oncol 23:6409-6414.

13.   Krause, J. R., and M. Shahidi-Asl. 2003. Molecular pathology in the diagnosis and treatment of non-Hodgkin's lymphomas. J Cell Mol Med 7:494-512.

14.   Lelbach, A., G. Muzes, and J. Feher. 2005. The insulin-like growth factor system: IGFs, IGF-binding proteins and IGFBP-proteases. Acta Physiol Hung 92:97-107.

15.   He, J., C. J. Rosen, D. J. Adams, and B. E. Kream. 2006. Postnatal growth and bone mass in mice with IGF-I haploinsufficiency. Bone 38:826-835.

16.   Rosen, C. J., and M. Pollak. 1999. Circulating IGF-I: New Perspectives for a New Century. Trends Endocrinol Metab 10:136-141.

17.   Rubin, J., X. Fan, J. Rahnert, B. Sen, C. L. Hsieh, T. C. Murphy, M. S. Nanes, L. G. Horton, W. G. Beamer, and C. J. Rosen. 2006. IGF-I secretion by prostate carcinoma cells does not alter tumor-bone cell interactions in vitro or in vivo. Prostate 66:789-800.

18.   Yakar, S., Y. Wu, J. Setser, and C. J. Rosen. 2002. The role of circulating IGF-I: lessons from human and animal models. Endocrine 19:239-248.

19. Yao, W., J. Zhong, C. J. Rosen, J. M. Hock, and W. H. Lee. 2005. Igf-I and postnatal growth of weaver mutant mice. Endocrine 26:117-125.

20. Bing-You, R. G., M. C. Denis, and C. J. Rosen. 1993. Low bone mineral density in adults with previous hypothalamic-pituitary tumors: correlations with serum growth hormone responses to GH-releasing hormone, insulin-like growth factor I, and IGF binding protein 3. Calcif Tissue Int 52:183-187.

21. Wang, J., J. Zhou, C. M. Cheng, J. J. Kopchick, and C. A. Bondy. 2004. Evidence supporting dual, IGF-I-independent and IGF-I-dependent, roles for GH in promoting longitudinal bone growth. J Endocrinol 180:247-255.

22. Jenkins, P. J., and S. A. Bustin. 2004. Evidence for a link between IGF-I and cancer. Eur J Endocrinol 151 Suppl 1:S17-22.

23. Borugian, M. J., J. J. Spinelli, Z. Sun, L. N. Kolonel, I. Oakley-Girvan, M. D. Pollak, A. S. Whittemore, A. H. Wu, and R. P. Gallagher. 2008. Prostate cancer risk in relation to insulin-like growth factor (IGF)-I and IGF-binding protein-3: a prospective multiethnic study. Cancer Epidemiol Biomarkers Prev 17:252-254.

24. Chen, T., A. Lukanova, K. Grankvist, A. Zeleniuch-Jacquotte, M. Wulff, R. Johansson, H. Schock, P. Lenner, G. Hallmans, G. Wadell, P. Toniolo, and E. Lundin. 2009. IGF-I during primiparous pregnancy and maternal risk of breast cancer. Breast Cancer Res Treat.

25. LeRoith, D., and C. T. Roberts, Jr. 2003. The insulin-like growth factor system and cancer. Cancer Lett 195:127-137.

26. Wu, Y., S. Yakar, L. Zhao, L. Hennighausen, and D. LeRoith. 2002. Circulating insulin-like growth factor-I levels regulate colon cancer growth and metastasis. Cancer Res 62:1030-1035.

27. Peters, G., S. Gongoll, C. Langner, M. Mengel, P. Piso, J. Klempnauer, J. Ruschoff, H. Kreipe, and R. von Wasielewski. 2003. IGF-1R, IGF-1 and IGF-2 expression as

potential prognostic and predictive markers in colorectal-cancer. Virchows Arch 443:139-145.

28.   Mairet-Coello, G., A. Tury, and E. DiCicco-Bloom. 2009. Insulin-like growth factor-1 promotes G(1)/S cell cycle progression through bidirectional regulation of cyclins and cyclin-dependent kinase inhibitors via the phosphatidylinositol 3-kinase/Akt pathway in developing rat cerebral cortex. J Neurosci 29:775-788.

29.   Rother, K. I., and D. Accili. 2000. Role of insulin receptors and IGF receptors in growth and development. Pediatr Nephrol 14:558-561.

30.   Werner, H., C. Hernandez-Sanchez, E. Karnieli, and D. Leroith. 1995. The regulation of IGF-I receptor gene expression. Int J Biochem Cell Biol 27:987-994.

31.   Shalita-Chesner, M., T. Glaser, and H. Werner. 2004. Signal transducer and activator of transcription-1 (STAT1), but not STAT5b, regulates IGF-I receptor gene expression in an osteosarcoma cell line. J Pediatr Endocrinol Metab 17:211-218.

32.   Yu, L., K. Saile, C. D. Swartz, H. He, X. Zheng, G. E. Kissling, X. Di, S. Lucas, S. J. Robboy, and D. Dixon. 2008. Differential expression of receptor tyrosine kinases (RTKs) and IGF-I pathway activation in human uterine leiomyomas. Mol Med 14:264-275.

33.   Kim, H., E. Barton, N. Muja, S. Yakar, P. Pennisi, and D. Leroith. 2005. Intact insulin and insulin-like growth factor-I receptor signaling is required for growth hormone effects on skeletal muscle growth and function in vivo. Endocrinology 146:1772-1779.

34.   Bentov, I., D. LeRoith, and H. Werner. 2003. The WT1 Wilms' tumor suppressor gene: a novel target for insulin-like growth factor-I action. Endocrinology 144:4276-4279.

35. Adams, T. E., V. C. Epa, T. P. Garrett, and C. W. Ward. 2000. Structure and function of the type 1 insulin-like growth factor receptor. Cell Mol Life Sci 57:1050-1093.

36. Chitnis, M. M., J. S. Yuen, A. S. Protheroe, M. Pollak, and V. M. Macaulay. 2008. The type 1 insulin-like growth factor receptor pathway. Clin Cancer Res 14:6364-6370.

37. Bertrand, F. E., L. S. Steelman, W. H. Chappell, S. L. Abrams, J. G. Shelton, E. R. White, D. L. Ludwig, and J. A. McCubrey. 2006. Synergy between an IGF-1R antibody and Raf/MEK/ERK and PI3K/Akt/mTOR pathway inhibitors in suppressing IGF-1R-mediated growth in hematopoietic cells. Leukemia 20:1254-1260.

38. Foulstone, E., S. Prince, O. Zaccheo, J. L. Burns, J. Harper, C. Jacobs, D. Church, and A. B. Hassan. 2005. Insulin-like growth factor ligands, receptors, and binding proteins in cancer. J Pathol 205:145-153.

39. Inagaki, K., A. Tiulpakov, P. Rubtsov, P. Sverdlova, V. Peterkova, S. Yakar, S. Terekhov, and D. LeRoith. 2007. A familial insulin-like growth factor-I receptor mutant leads to short stature: clinical and biochemical characterization. J Clin Endocrinol Metab 92:1542-1548.

40. Sadagurski, M., S. Yakar, G. Weingarten, M. Holzenberger, C. J. Rhodes, D. Breitkreutz, D. Leroith, and E. Wertheimer. 2006. Insulin-like growth factor 1 receptor signaling regulates skin development and inhibits skin keratinocyte differentiation. Mol Cell Biol 26:2675-2687.

41. Scavo, L. M., M. Karas, M. Murray, and D. Leroith. 2004. Insulin-like growth factor-I stimulates both cell growth and lipogenesis during differentiation of human mesenchymal stem cells into adipocytes. J Clin Endocrinol Metab 89:3543-3553.

42. Liu, J. P., J. Baker, A. S. Perkins, E. J. Robertson, and A. Efstratiadis. 1993. Mice carrying null mutations of the genes encoding insulin-like growth factor I (Igf-1) and type 1 IGF receptor (Igf1r). Cell 75:59-72.

43. Rosen, C. J., C. L. Ackert-Bicknell, M. L. Adamo, K. L. Shultz, J. Rubin, L. R. Donahue, L. G. Horton, K. M. Delahunty, W. G. Beamer, J. Sipos, D. Clemmons, T. Nelson, M. L. Bouxsein, and M. Horowitz. 2004. Congenic mice with low serum IGF-I have increased body fat, reduced bone mineral density, and an altered osteoblast differentiation program. Bone 35:1046-1058.

44. Rosen, C. J., H. P. Dimai, D. Vereault, L. R. Donahue, W. G. Beamer, J. Farley, S. Linkhart, T. Linkhart, S. Mohan, and D. J. Baylink. 1997. Circulating and skeletal insulin-like growth factor-I (IGF-I) concentrations in two inbred strains of mice with different bone mineral densities. Bone 21:217-223.

45. Wu, Y., H. Sun, S. Yakar, and D. LeRoith. 2009. Elevated levels of insulin-like growth factor (IGF)-I in serum rescue the severe growth retardation of IGF-I null mice. Endocrinology 150:4395-4403.

46. Gualberto, A., and M. Pollak. 2009. Clinical Development of Inhibitors of the Insulin-like Growth Factor Receptor in Oncology. Curr Drug Targets.

47. Gualco, E., J. Y. Wang, L. Del Valle, K. Urbanska, F. Peruzzi, K. Khalili, S. Amini, and K. Reiss. 2009. IGF-IR in neuroprotection and brain tumors. Front Biosci 14:352-375.

48. LeRoith, D., R. Baserga, L. Helman, and C. T. Roberts, Jr. 1995. Insulin-like growth factors and cancer. Ann Intern Med 122:54-59.

49. Macaulay, V. M. 1992. Insulin-like growth factors and cancer. Br J Cancer 65:311-320.

50.   Mitsiades, C. S., and N. Mitsiades. 2005. Treatment of hematologic malignances and solid tumors by inhibiting IGF receptor signaling. Expert Rev Anticancer Ther 5:487-499.

51.   Moore, T., S. Carbajal, L. Beltran, S. N. Perkins, S. Yakar, D. Leroith, S. D. Hursting, and J. Digiovanni. 2008. Reduced susceptibility to two-stage skin carcinogenesis in mice with low circulating insulin-like growth factor I levels. Cancer Res 68:3680-3688.

52.   Pandini, G., R. Vigneri, A. Costantino, F. Frasca, A. Ippolito, Y. Fujita-Yamaguchi, K. Siddle, I. D. Goldfine, and A. Belfiore. 1999. Insulin and insulin-like growth factor-I (IGF-I) receptor overexpression in breast cancers leads to insulin/IGF-I hybrid receptor overexpression: evidence for a second mechanism of IGF-I signaling. Clin Cancer Res 5:1935-1944.

53.   Pollak, M. 2008. Insulin and insulin-like growth factor signalling in neoplasia. Nat Rev Cancer 8:915-928.

54.   Pollak, M. 2008. Targeting insulin and insulin-like growth factor signalling in oncology. Curr Opin Pharmacol 8:384-392.

55.   Samani, A. A., S. Yakar, D. LeRoith, and P. Brodt. 2007. The role of the IGF system in cancer growth and metastasis: overview and recent insights. Endocr Rev 28:20-47.

56.   Wolpin, B. M., J. A. Meyerhardt, A. T. Chan, K. Ng, J. A. Chan, K. Wu, M. N. Pollak, E. L. Giovannucci, and C. S. Fuchs. 2009. Insulin, the insulin-like growth factor axis, and mortality in patients with nonmetastatic colorectal cancer. J Clin Oncol 27:176-185.

57.   Yu, H., and T. Rohan. 2000. Role of the insulin-like growth factor family in cancer development and progression. J Natl Cancer Inst 92:1472-1489.

58.   Jones, R. A., C. I. Campbell, J. J. Petrik, and R. A. Moorehead. 2008.

Characterization of a novel primary mammary tumor cell line reveals that cyclin D1

is regulated by the type I insulin-like growth factor receptor. Mol Cancer Res 6:819-

828.

59.   Rubini, M., A. Hongo, C. D'Ambrosio, and R. Baserga. 1997. The IGF-I receptor in

mitogenesis and transformation of mouse embryo cells: role of receptor number.

Exp Cell Res 230:284-292.

60.   Zhang, D., A. A. Samani, and P. Brodt. 2003. The role of the IGF-I receptor in the

regulation of matrix metalloproteinases, tumor invasion and metastasis. Horm Metab

Res 35:802-808.

61.   Flossmann-Kast, B. B., P. M. Jehle, A. Hoeflich, G. Adler, and M. P. Lutz. 1998. Src

stimulates insulin-like growth factor I (IGF-I)-dependent cell proliferation by

increasing IGF-I receptor number in human pancreatic carcinoma cells. Cancer Res

58:3551-3554.

62.   Dupont, J., M. Karas, and D. LeRoith. 2000. The potentiation of estrogen on insulin-

like growth factor I action in MCF-7 human breast cancer cells includes cell cycle

components. J Biol Chem 275:35893-35901.

63.   Lann, D., and D. LeRoith. 2008. The role of endocrine insulin-like growth factor-I

and insulin in breast cancer. J Mammary Gland Biol Neoplasia 13:371-379.

64.   Sciacca, L., A. Costantino, G. Pandini, R. Mineo, F. Frasca, P. Scalia, P. Sbraccia, I.

D. Goldfine, R. Vigneri, and A. Belfiore. 1999. Insulin receptor activation by IGF-II in

breast cancers: evidence for a new autocrine/paracrine mechanism. Oncogene

18:2471-2479.

65.   Shukla, V., X. Coumoul, L. Cao, R. H. Wang, C. Xiao, X. Xu, S. Ando, S. Yakar, D.

Leroith, and C. Deng. 2006. Absence of the full-length breast cancer-associated

gene-1 leads to increased expression of insulin-like growth factor signaling axis members. Cancer Res 66:7151-7157.

66.   Monti, S., L. Proietti-Pannunzi, A. Sciarra, F. Lolli, P. Falasca, M. Poggi, F. S. Celi, and V. Toscano. 2007. The IGF axis in prostate cancer. Curr Pharm Des 13:719-727.

67.   Mitsiades, C. S., N. S. Mitsiades, C. J. McMullan, V. Poulaki, R. Shringarpure, M. Akiyama, T. Hideshima, D. Chauhan, M. Joseph, T. A. Libermann, C. Garcia-Echeverria, M. A. Pearson, F. Hofmann, K. C. Anderson, and A. L. Kung. 2004. Inhibition of the insulin-like growth factor receptor-1 tyrosine kinase activity as a therapeutic strategy for multiple myeloma, other hematologic malignancies, and solid tumors. Cancer Cell 5:221-230.

68.   Chng, W. J., A. Gualberto, and R. Fonseca. 2006. IGF-1R is overexpressed in poor-prognostic subtypes of multiple myeloma. Leukemia 20:174-176.

69.   Dupont, J., A. Pierre, P. Froment, and C. Moreau. 2003. The insulin-like growth factor axis in cell cycle progression. Horm Metab Res 35:740-750.

70.   Hamelers, I. H., R. F. van Schaik, J. Sipkema, J. S. Sussenbach, and P. H. Steenbergh. 2002. Insulin-like growth factor I triggers nuclear accumulation of cyclin D1 in MCF-7S breast cancer cells. J Biol Chem 277:47645-47652.

71.   Muise-Helmericks, R. C., H. L. Grimes, A. Bellacosa, S. E. Malstrom, P. N. Tsichlis, and N. Rosen. 1998. Cyclin D expression is controlled post-transcriptionally via a phosphatidylinositol 3-kinase/Akt-dependent pathway. J Biol Chem 273:29864-29872.

72.   Furlanetto, R. W., S. E. Harwell, and K. K. Frick. 1994. Insulin-like growth factor-I induces cyclin-D1 expression in MG63 human osteosarcoma cells in vitro. Mol Endocrinol 8:510-517.

73. Coats, S., W. M. Flanagan, J. Nourse, and J. M. Roberts. 1996. Requirement of p27Kip1 for restriction point control of the fibroblast cell cycle. Science 272:877-880.

74. Datta, S. R., H. Dudek, X. Tao, S. Masters, H. Fu, Y. Gotoh, and M. E. Greenberg. 1997. Akt phosphorylation of BAD couples survival signals to the cell-intrinsic death machinery. Cell 91:231-241.

75. Hanahan, D., and R. A. Weinberg. 2000. The hallmarks of cancer. Cell 100:57-70.

76. Adachi, Y., C. T. Lee, K. Coffee, N. Yamagata, J. E. Ohm, K. H. Park, M. M. Dikov, S. R. Nadaf, C. L. Arteaga, and D. P. Carbone. 2002. Effects of genetic blockade of the insulin-like growth factor receptor in human colon cancer cell lines. Gastroenterology 123:1191-1204.

77. Burfeind, P., C. L. Chernicky, F. Rininsland, and J. Ilan. 1996. Antisense RNA to the type I insulin-like growth factor receptor suppresses tumor growth and prevents invasion by rat prostate cancer cells in vivo. Proc Natl Acad Sci U S A 93:7263-7268.

78. Cohen, B. D., D. A. Baker, C. Soderstrom, G. Tkalcevic, A. M. Rossi, P. E. Miller, M. W. Tengowski, F. Wang, A. Gualberto, J. S. Beebe, and J. D. Moyer. 2005. Combination therapy enhances the inhibition of tumor growth with the fully human anti-type 1 insulin-like growth factor receptor monoclonal antibody CP-751,871. Clin Cancer Res 11:2063-2073.

79. Dunn, S. E., M. Ehrlich, N. J. Sharp, K. Reiss, G. Solomon, R. Hawkins, R. Baserga, and J. C. Barrett. 1998. A dominant negative mutant of the insulin-like growth factor-I receptor inhibits the adhesion, invasion, and metastasis of breast cancer. Cancer Res 58:3353-3361.

80. Gualberto, A., and M. Pollak. 2009. Emerging role of insulin-like growth factor receptor inhibitors in oncology: early clinical trial results and future directions. Oncogene 28:3009-3021.

81. Lee, C. T., K. H. Park, Y. Adachi, J. Y. Seol, C. G. Yoo, Y. W. Kim, S. K. Han, Y. S. Shim, K. Coffee, M. M. Dikov, and D. P. Carbone. 2003. Recombinant adenoviruses expressing dominant negative insulin-like growth factor-I receptor demonstrate antitumor effects on lung cancer. Cancer Gene Ther 10:57-63.

82. Moschos, S. J., and C. S. Mantzoros. 2002. The role of the IGF system in cancer: from basic to clinical studies and clinical applications. Oncology 63:317-332.

83. Feng, Y., and D. S. Dimitrov. 2008. Monoclonal antibodies against components of the IGF system for cancer treatment. Curr Opin Drug Discov Devel 11:178-185.

84. Girnita, A., L. Girnita, F. del Prete, A. Bartolazzi, O. Larsson, and M. Axelson. 2004. Cyclolignans as inhibitors of the insulin-like growth factor-1 receptor and malignant cell growth. Cancer Res 64:236-242.

85. Economou, M. A., S. Andersson, D. Vasilcanu, C. All-Ericsson, E. Menu, A. Girnita, L. Girnita, M. Axelson, S. Seregard, and O. Larsson. 2008. Oral picropodophyllin (PPP) is well tolerated in vivo and inhibits IGF-1R expression and growth of uveal melanoma. Invest Ophthalmol Vis Sci 49:2337-2342.

86. Economou, M. A., J. Wu, D. Vasilcanu, L. Rosengren, C. All-Ericsson, I. van der Ploeg, E. Menu, L. Girnita, M. Axelson, O. Larsson, S. Seregard, and A. Kvanta. 2008. Inhibition of VEGF secretion and experimental choroidal neovascularization by picropodophyllin (PPP), an inhibitor of the insulin-like growth factor-1 receptor. Acta Ophthalmol 86 Thesis 4:42-49.

87. Menu, E., H. Jernberg-Wiklund, T. Stromberg, H. De Raeve, L. Girnita, O. Larsson, M. Axelson, K. Asosingh, K. Nilsson, B. Van Camp, and K. Vanderkerken. 2006. Inhibiting the IGF-1 receptor tyrosine kinase with the cyclolignan PPP: an in vitro and in vivo study in the 5T33MM mouse model. Blood 107:655-660.

88. Vasilcanu, R., D. Vasilcanu, L. Rosengren, N. Natalishvili, B. Sehat, S. Yin, A. Girnita, M. Axelson, L. Girnita, and O. Larsson. 2008. Picropodophyllin induces

downregulation of the insulin-like growth factor 1 receptor: potential mechanistic involvement of Mdm2 and beta-arrestin1. Oncogene 27:1629-1638.

89.   Rodon, J., V. DeSantos, R. J. Ferry, Jr., and R. Kurzrock. 2008. Early drug development of inhibitors of the insulin-like growth factor-I receptor pathway: lessons from the first clinical trials. Mol Cancer Ther 7:2575-2588.

90.   Vasilcanu, D., A. Girnita, L. Girnita, R. Vasilcanu, M. Axelson, and O. Larsson. 2004. The cyclolignan PPP induces activation loop-specific inhibition of tyrosine phosphorylation of the insulin-like growth factor-1 receptor. Link to the phosphatidyl inositol-3 kinase/Akt apoptotic pathway. Oncogene 23:7854-7862.

91.   Economou, M. A., S. Andersson, D. Vasilcanu, C. All-Ericsson, E. Menu, A. Girnita, L. Girnita, M. Axelson, S. Seregard, and O. Larsson. 2008. Oral picropodophyllin (PPP) is well tolerated in vivo and inhibits IGF-1R expression and growth of uveal melanoma. Acta Ophthalmol 86 Thesis 4:35-41.

92.   Favelyukis, S., J. H. Till, S. R. Hubbard, and W. T. Miller. 2001. Structure and autoregulation of the insulin-like growth factor 1 receptor kinase. Nat Struct Biol 8:1058-1063.

93.   Stromberg, T., S. Ekman, L. Girnita, L. Y. Dimberg, O. Larsson, M. Axelson, J. Lennartsson, U. Hellman, K. Carlson, A. Osterborg, K. Vanderkerken, K. Nilsson, and H. Jernberg-Wiklund. 2006. IGF-1 receptor tyrosine kinase inhibition by the cyclolignan PPP induces G2/M-phase accumulation and apoptosis in multiple myeloma cells. Blood 107:669-678.

94.   Guo, Y. Q., and S. L. Chen. 2006. [The significance of IGF-1, VEGF, IL-6 in multiple myeloma progression]. Zhonghua Xue Ye Xue Za Zhi 27:231-234.

95.   Tonra, J. R., E. Corcoran, D. S. Deevi, P. Steiner, J. Kearney, H. Li, D. L. Ludwig, Z. Zhu, L. Witte, D. Surguladze, and D. J. Hicklin. 2009. Prioritization of EGFR/IGF-

IR/VEGFR2 combination targeted therapies utilizing cancer models. Anticancer Res 29:1999-2007.

96.   Bataille, R., N. Robillard, H. Avet-Loiseau, J. L. Harousseau, and P. Moreau. 2005. CD221 (IGF-1R) is aberrantly expressed in multiple myeloma, in relation to disease severity. Haematologica 90:706-707.

97.   Freund, G. G., D. T. Kulas, and R. A. Mooney. 1993. Insulin and IGF-1 increase mitogenesis and glucose metabolism in the multiple myeloma cell line, RPMI 8226. J Immunol 151:1811-1820.

98.   Jernberg-Wiklund, H., and K. Nilsson. 2007. Control of apoptosis in human multiple myeloma by insulin-like growth factor I (IGF-I). Adv Cancer Res 97:139-165.

99.   Menu, E., H. Jernberg-Wiklund, H. De Raeve, E. De Leenheer, L. Coulton, O. Gallagher, E. Van Valckenborgh, O. Larsson, M. Axelson, K. Nilsson, B. Van Camp, P. Croucher, and K. Vanderkerken. 2007. Targeting the IGF-1R using picropodophyllin in the therapeutical 5T2MM mouse model of multiple myeloma: beneficial effects on tumor growth, angiogenesis, bone disease and survival. Int J Cancer 121:1857-1861.

100.   Mitsiades, C. S., N. Mitsiades, V. Poulaki, R. Schlossman, M. Akiyama, D. Chauhan, T. Hideshima, S. P. Treon, N. C. Munshi, P. G. Richardson, and K. C. Anderson. 2002. Activation of NF-kappaB and upregulation of intracellular anti-apoptotic proteins via the IGF-1/Akt signaling in human multiple myeloma cells: therapeutic implications. Oncogene 21:5673-5683.

101.   Shi, P., J. Chandra, X. Sun, M. Gergely, J. E. Cortes, G. Garcia-Manero, R. B. Arlinghaus, R. Lai, and H. M. Amin. 2009. Inhibition of IGF-IR tyrosine kinase induces apoptosis and cell cycle arrest in imatinib-resistant chronic myeloid leukemia cells. J Cell Mol Med.

102.   Shi, P., R. Lai, Q. Lin, A. S. Iqbal, L. C. Young, L. W. Kwak, R. J. Ford, and H. M. Amin. 2009. IGF-IR tyrosine kinase interacts with NPM-ALK oncogene to induce survival of T-cell ALK+ anaplastic large-cell lymphoma cells. Blood 114:360-370.

103.   Amin, H. M., T. J. McDonnell, L. J. Medeiros, G. Z. Rassidakis, V. Leventaki, S. L. O'Connor, M. J. Keating, and R. Lai. 2003. Characterization of 4 mantle cell lymphoma cell lines. Arch Pathol Lab Med 127:424-431.

104.   Pietrzkowski, Z., C. Sell, R. Lammers, A. Ullrich, and R. Baserga. 1992. Roles of insulinlike growth factor 1 (IGF-1) and the IGF-1 receptor in epidermal growth factor-stimulated growth of 3T3 cells. Mol Cell Biol 12:3883-3889.

105.   Sell, C., M. Rubini, R. Rubin, J. P. Liu, A. Efstratiadis, and R. Baserga. 1993. Simian virus 40 large tumor antigen is unable to transform mouse embryonic fibroblasts lacking type 1 insulin-like growth factor receptor. Proc Natl Acad Sci U S A 90:11217-11221.

106.   Stewart, A. J., M. D. Johnson, F. E. May, and B. R. Westley. 1990. Role of insulin-like growth factors and the type I insulin-like growth factor receptor in the estrogen-stimulated proliferation of human breast cancer cells. J Biol Chem 265:21172-21178.

107.   Bergmann, U., H. Funatomi, M. Yokoyama, H. G. Beger, and M. Korc. 1995. Insulin-like growth factor I overexpression in human pancreatic cancer: evidence for autocrine and paracrine roles. Cancer Res 55:2007-2011.

108.   Gupta, S., T. Barrett, A. J. Whitmarsh, J. Cavanagh, H. K. Sluss, B. Derijard, and R. J. Davis. 1996. Selective interaction of JNK protein kinase isoforms with transcription factors. EMBO J 15:2760-2770.

109.   Walsh, P. T., L. M. Smith, and R. O'Connor. 2002. Insulin-like growth factor-1 activates Akt and Jun N-terminal kinases (JNKs) in promoting the survival of T lymphocytes. Immunology 107:461-471.

110. Miyazaki, T., and S. Arai. 2007. Two distinct controls of mitotic cdk1/cyclin B1 activity requisite for cell growth prior to cell division. Cell Cycle 6:1419-1425.

111. Wu, J. D., A. Odman, L. M. Higgins, K. Haugk, R. Vessella, D. L. Ludwig, and S. R. Plymate. 2005. In vivo effects of the human type I insulin-like growth factor receptor antibody A12 on androgen-dependent and androgen-independent xenograft human prostate tumors. Clin Cancer Res 11:3065-3074.

Vita

Deeksha Vishwamitra was raised in Cincinnati, OH, the Daughter of Nimi Vishwamitra and Teju Vishwamitra. After completing her work at Indian Hill High School, Cincinnati, OH in 2003, she entered Ohio State University in Columbus, OH. She received the degree of Bachelor of Science with a major in Molecular Genetics from OSU in June 2007. In August of 2007 she entered The University of Texas Health Science Center at Houston Graduate School of Biomedical Sciences.

Permanent address:
4605 N. Braeswood, Apt. 216
Houston, Texas 77096